J Pharmacol Sci 101, 144 – 150 (2006)

Journal of Pharmacological Sciences

Full Paper

Heterotrimeric G Protein $G\alpha_{13}$-Induced Induction of Cytokine mRNAs Through Two Distinct Pathways in Cardiac Fibroblasts

Yuichi Nagamatsu[1], Motohiro Nishida[1], Naoya Onohara[1], Masashi Fukutomi[1], Yoshiko Maruyama[2], Hiroyuki Kobayashi[1], Yoji Sato[3], and Hitoshi Kurose[1,*]

[1]*Department of Pharmacology and Toxicology, Graduate School of Pharmaceutical Sciences, Kyushu University, Fukuoka 812-8582, Japan*
[2]*Laboratory of Cellular Signaling, Graduate School of Pharmaceutical Sciences, University of Tokyo, Tokyo 113-0033, Japan*
[3]*National Institute of Health Sciences, Tokyo 158-8501, Japan*

Received December 14, 2005; Accepted April 17, 2006

Abstract. Overexpression of constitutively active (CA)-$G\alpha_{13}$ significantly increased the expression of interleukin (IL)-1β and IL-6 mRNAs and proteins in rat cardiac fibroblasts. IL-1β mRNA induction by CA-$G\alpha_{13}$ was suppressed by diphenyleneiodonium (DPI), an NADPH oxidase inhibitor, but not by BAPTA-AM, an intracellular Ca^{2+} chelator. In contrast, IL-6 mRNA induction by CA-$G\alpha_{13}$ was suppressed by BAPTA-AM but not by DPI. However, both IL-1β and IL-6 mRNA induction was suppressed by nuclear factor κB (NF-κB) inhibitors. The CA-$G\alpha_{13}$-induced NF-κB activation was suppressed by DPI and BAPTA-AM, but not C3 toxin and the Rho-kinase inhibitor Y27632. IL-6 mRNA induction by CA-$G\alpha_{13}$ was suppressed by SK&F96365 (1-[β-[3-(4-methoxyphenyl)propoxy]-4-methoxyphenethyl]-1*H*-imidazole hydrochloride), an inhibitor of receptor-activated nonselective cation channels, and the expression of CA-$G\alpha_{13}$ increased basal Ca^{2+} influx. These results suggest that $G\alpha_{13}$ regulates IL-1β mRNA induction through the reactive oxygen species-NF-κB pathway, while it regulates IL-6 mRNA induction through the Ca^{2+}-NF-κB pathway.

Keywords: cardiac fibroblast, $G\alpha_{13}$ protein, nuclear factor of κB, Ca^{2+}, interleukin

Introduction

Cardiac fibroblasts play a central role in maintaining extracellular matrix in the normal heart (1). These cells also mediate inflammatory and fibrotic myocardial remodeling in the injured and failing heart. Cardiac fibroblasts serve as intermediate sensors and amplifiers of signals from immune cells and myocytes through production of autocrine and paracrine mediators such as cytokines, growth factors, prostaglandins, and nitric oxide (1 – 5). These mediators induce cardiac hypertrophy and transition of cardiomyocytes to fibroblast phenotype, causing cardiac dysfunction (1, 2).

Interleukins, such as interleukin-1β (IL-1β) or IL-6, are humoral factors that elicit hypertrophy of cardiomyocytes and hyperplasia of cardiac fibroblasts (4 – 9). In these cells, receptor stimulation such as angiotensin (Ang) II (8) or endothelin-1 (9) increases IL-6 expression, and stimulation of β-adrenergic receptor (4) or 5-hydroxytryptamine 2B (5-HT_{2B}) receptor (5) increases IL-1β. These cytokines regulate phenotype and functions of the heart in autocrine and paracrine manners. Recent studies have suggested that these indirect actions are the major mechanism by which Ang II controls cardiac fibroblasts (2, 8). We have previously reported that stimulation of Ang II receptor activates the α subunit of heterotrimeric $G_{12/13}$ proteins ($G\alpha_{12/13}$), leading to production of reactive oxygen species (ROS) through Rac-dependent activation of NADPH oxidase and that $G\alpha_{12/13}$ mediate activation of nuclear factor of activated T cells (NFAT) in rat cardiac fibroblasts (10). As NFAT is reported to regulate IL-6 mRNA induction in vascular smooth muscle cells (11), $G\alpha_{12/13}$ signaling is

*Corresponding author. kurose@phar.kyushu-u.ac.jp
Published online in J-STAGE: June 15, 2006
doi: 10.1254/jphs.FP0051036

assumed to participate in induction of cytokine mRNA in cardiac fibroblasts. However, it has not been examined whether $G\alpha_{12/13}$ actually regulate cytokine mRNA induction in cardiac fibroblasts.

The G_{12} family G proteins, G_{12} and G_{13}, couple with various G protein-coupled receptors and mediate physiological responses by interacting with different signaling proteins (12). The involvement of $G\alpha_{12/13}$ in cardiac hypertrophy by receptor stimulation has been well recognized as the stimulation of α_1-adrenergic receptor (13), endothelin-1 receptor (14), or Ang II receptor (15) induces hypertrophy through $G\alpha_{12/13}$-dependent activation of c-Jun NH_2-terminal kinase (JNK). However, the physiological role of $G\alpha_{12/13}$ signaling in cardiac fibroblasts has not been established.

In this study, we examine whether $G\alpha_{12/13}$ participate in the induction of IL-1β and IL-6 mRNAs in cardiac fibroblasts by expressing constitutively active (CA) mutants of $G\alpha_{12}$ and $G\alpha_{13}$. This study is the first report to demonstrate that activated $G\alpha_{13}$, but not $G\alpha_{12}$, increases IL-1β and IL-6 mRNAs expression through NF-κB-dependent, but Rho-independent mechanisms in cardiac fibroblasts. We further demonstrate that IL-1β mRNA induction by CA-$G\alpha_{13}$ requires ROS, and IL-6 mRNA induction by CA-$G\alpha_{13}$ requires the increase in basal Ca^{2+} influx.

Materials and Methods

Materials and recombinant adenoviruses

BAPTA-AM, cyclosporine A, and Y27632 were purchased from Calbiochem-Novabiochem Co. (San Diego, CA, USA). Catalase, diphenyleneiodonium (DPI), and 1-[β-[3-(4-methoxyphenyl)propoxy]-4-methoxyphenethyl]-1*H*-imidazole hydrochloride (SK&F96365) were purchased from Sigma-Aldrich (St. Louis, MO, USA). 6-(Phenylsulfinyl)tetrazolo[1,5-*b*] pyridazine (Ro-106-9920) was from Tocris Cookson, Ltd. (Bristol, UK). Dulbecco's Modified Eagle's medium (DMEM) and penicillin/streptomycin were from Invitrogen Co. (Carlsbad, CA, USA) Fura2/AM was from Dojindo (Kumamoto). Collagenase and FuGENE 6 were from Roche Diagnostics (Mannheim, Germany). Dual-luciferase Reagents were from Promega Co. (Madison, WI, USA). pNF (nuclear factor)-κB-Luc and pRL-SV40 were from Stratagene Co. (La Jolla, CA, USA) Recombinant adenoviruses of CA-$G\alpha_q$ (R183C), CA-$G\alpha_{12}$ (Q229L), CA-$G\alpha_{13}$ (Q226L), C3 toxin, and IκBα mutant were produced as described previously (10, 15).

Cell culture

Cardiac fibroblasts were prepared from ventricles of 1 – 2-day-old Sprague-Dawley rats, as described previously (16). Briefly, after digestion of ventricles with 0.1% collagenase, isolated fibroblasts were plated on a non-coated dish in DMEM containing 10% fetal bovine serum and 50 U/ml penicillin/streptomycin. Sub-confluent cells were serum-starved for 48 h and used for the experiments.

Measurement of IL-1β and IL-6 mRNAs expression

Three hours after adenoviral infection (300 multiplicity of infection (MOI)) in serum-free medium, fibroblasts (3×10^5 cells) in 6 well dishes were treated with the chemical inhibitors indicated in the figures. Total RNA was extracted 36 h after infection with RNeasy Mini Kit (Qiagen, Inc., Valencia, CA, USA) and RNase-free DNase set (Qiagen), and then 150 ng (in the case of IL-1β and IL-6) or 5 pg (in the case of 18 S rRNA) of total RNA was subjected to real-time reverse transcriptase PCR (RT-PCR) for quantitative measurement. Oligonucleotide primers and fluorescent-labeled TaqMan® probes were designed with Primer Express software (Applied Biosystems, Foster City, CA, USA). IL-1β (forward primer, 5'-GATGATGACGACCTGCTAGTG TGT-3'; reverse primer, 5'-GACAGCACGAGGCAT TTTTGT-3'; TaqMan® probe, 5'-ATTAGACAGCTG CACTGCAGGCTTCGAGAT-3'), IL-6 (forward primer, 5'-CAACTTCCAATGCTCTCCTAATGG-3'; reverse primer, 5'-CCGAGTAGACCTCATAGTGACC TTT-3'; TaqMan® probe, 5'-TCACAGAAGGAGTGG CTAAGGACCAAGACC-3'), TaqMan® 18 S rRNA primers, and a 5'-VIC™-labelled probe were used according to the manufacturer's instructions (Applied Biosystems). All reactions were performed in TaqMan® One-Step RT-PCR Master Mix Reagents (Applied Biosystems) and the Applied Biosystems 7500 Real-Time PCR System (Applied Biosystems). The 18 S ribosomal RNA was used as an internal control to normalize the differences in the amount of total RNA in each sample.

ELISA for IL-1β and IL-6

ELISA kits for Rat IL-1β and IL-6 were purchased from Pierce (Rockford, IL, USA) and Immuno-Biological Laboratories (Hamburg, Germany), respectively. Assays were performed according to the manufacturer's instructions.

Measurement of NF-κB activation

Two hours after adenoviral infection (100 MOI) in serum-free medium, fibroblasts (3×10^5 cells) in 24-well dishes were transiently co-transfected with 0.45 μg pNF-κB-Luc and 0.05 μg pRL-SV40 control plasmid, using Fugene 6 (10). Luciferase activity was measured 48 h after transfection with Dual-luciferase Reagents.

Intracellular Ca^{2+} measurement

The intracellular Ca^{2+} concentration ($[Ca^{2+}]_i$) of cardiac fibroblasts was determined by the previously described method (10). Briefly, cells (1×10^5) were plated on glass-bottom, 35-mm dish and were loaded with 1 μM fura-2/AM in the cultured medium at 37°C for 30 min. The cells were washed with Tyrode solution containing 118 mM NaCl, 5.4 mM KCl, 2 mM $CaCl_2$, 2 mM $MgCl_2$, 10 mM Hepes (pH 7.4), 0.33 mM NaH_2PO_4, 10 mM glucose, and 30 mM taurine. Fluorescence images of GFP-positive cells were recorded and analyzed with a video image analysis system (Aquacosmos, Hamamatsu Photonics Co., Shizuoka). Resting $[Ca^{2+}]_i$ levels in CA-Gα_{13}-expressing cells were similar (60 – 90 nM) to GFP-expressing cells as analyzed by in vivo calibration.

Statistical analyses

The results are presented as the mean ± S.E.M. The data were accumulated under each condition from at least three independent experiments. For the measurement of $[Ca^{2+}]_i$, data of time course experiments were plotted from one of three similar experiments that were performed with more than 30 cells. The *P* values are the results of one way ANOVA followed by Bonferroni's *t*-test. In the ELISA assay, the *P* values are the results of Student's *t*-test.

Results

Activated Gα_{13} increases IL-1β and IL-6 mRNAs expression in cardiac fibroblasts

To examine whether G proteins are involved in cytokine production in cardiac fibroblasts, various CA mutants of Gα were expressed at 300 MOI. Among the various CA mutants, CA-Gα_{13} increased IL-1β mRNA expression by 6.3-fold and IL-6 mRNA expression by 15-fold, compared to LacZ-expressing cells (Fig. 1). The expression of CA-Gα_{12} did not increase IL-1β and IL-6 mRNAs. Although CA-Gα_q significantly increased IL-1β mRNA expression, the increase in IL-6 mRNA expression by CA-Gα_q was not significant. These results suggest that Gα_{13} predominantly regulates the induction of IL-1β and IL-6 mRNAs in cardiac fibroblasts.

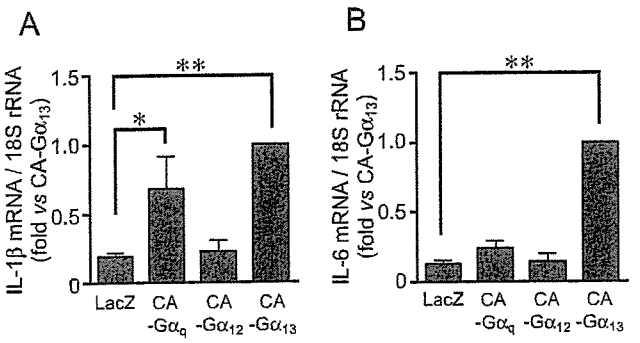

Fig. 1. Activated Gα_{13} increases IL-1β and IL-6 mRNAs expression in cardiac fibroblasts. Cells were infected with LacZ, CA-Gα_q, CA-Gα_{12}, or CA-Gα_{13} at 300 MOI, and IL-1β (A) and IL-6 (B) mRNAs expression were determined (n = 11). The fold increases were calculated by the values of CA-Gα_{13}-expressing cells set as 1. *P<0.05, **P<0.01 *vs* LacZ-expressing cells.

Involvement of NF-κB in activated Gα_{13}-induced cytokine mRNA induction

It has been reported that the promoter regions of IL-1β and IL-6 contain a putative NF-κB binding site (17, 18). Thus, we next examined whether NF-κB is involved in CA-Gα_{13}-induced expression of IL-1β and IL-6 mRNAs in cardiac fibroblasts. The induction of IL-1β and IL-6 mRNAs by CA-Gα_{13} was significantly suppressed by

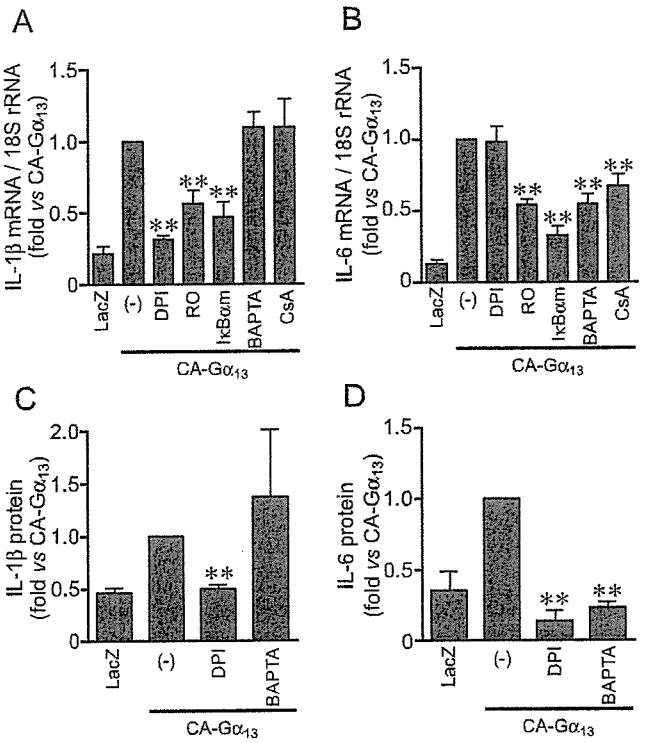

Fig. 2. Involvement of NF-κB, NFAT, ROS, or Ca^{2+} in the induction of IL-1β and IL-6 mRNAs and proteins by Gα_{13} activation. A, B: Cardiac fibroblasts were infected with LacZ and CA-Gα_{13} at 300 MOI or co-infected with CA-Gα_{13} at 300 MOI and IκBαm at 100 MOI. Three hours after infection, cells were treated for 33 h with 3 μM DPI, 4 μM Ro-106-9920 (RO), 3 μM BAPTA-AM (BAPTA), or 500 ng/ml cyclosporine A (CsA), and IL-1β (A) or IL-6 (B) mRNA expression were determined (n = 3 – 6). C, D: Three hours after infection of CA-Gα_{13} at 300 MOI, cells were treated for 33 h with 3 μM DPI or 3 μM BAPTA, and the concentration of IL-1β (C) or IL-6 (D) protein in cultured medium were determined by ELISA assay (n = 3). The fold increases were calculated by the values of CA-Gα_{13}-expressing cells set as 1. **P<0.01 *vs* CA-Gα_{13}-expressing cells.

treatment with 4 μM Ro-106-9920, a selective inhibitor of IκB phosphorylation, or by the expression of a non-phosphorylated form of IκBα (IkBαm) at 100 MOI (Fig. 2). These results suggest that NF-κB regulates the induction of IL-1β and IL-6 mRNAs by CA-$G\alpha_{13}$.

Involvement of Ca^{2+} in the induction of IL-6 mRNA and protein by $G\alpha_{13}$ activation

Abbott et al. reported that NFAT functions as a cofactor of NF-κB signaling, leading to IL-6 mRNA induction by ATP receptor stimulation in vascular smooth muscle cells (11). We have previously demonstrated that the expression of CA-$G\alpha_{13}$ induces NFAT activation in cardiac fibroblasts (10). As NFAT activity is exclusively regulated by $[Ca^{2+}]_i$, we investigated the involvement of Ca^{2+} in CA-$G\alpha_{13}$-induced mRNA expression of IL-1β and IL-6. Treatment with 3 μM BAPTA-AM, an intracellular Ca^{2+} chelator, significantly suppressed IL-6 mRNA induction by CA-$G\alpha_{13}$, but not IL-1β mRNA induction (Fig. 2: A and B). In addition, the treatment with 500 ng/ml cyclosporine A, an inhibitor of calcineurin, also suppressed IL-6 mRNA induction by CA-$G\alpha_{13}$. However, cyclosporine A did not affect IL-1β mRNA induction by CA-$G\alpha_{13}$. As shown in Fig. 2, C and D, the expression of CA-$G\alpha_{13}$ increased the amounts of IL-1β in cultured medium by 2.2-fold (from 11.5 to 24.9 pg/ml) and IL-6 by 2.8-fold (from 8.7 to 24.7 pg/ml), compared to LacZ-expressing cells. Treatment with 3 μM BAPTA-AM completely suppressed the induction of IL-6 protein by CA-$G\alpha_{13}$, but not the induction of IL-1β protein. Furthermore, 3 μM BAPTA-AM significantly suppressed CA-$G\alpha_{13}$-induced NF-κB activation (Fig. 3). These results suggest that Ca^{2+}-dependent NFAT and NF-κB activation by $G\alpha_{13}$ activation mediates the induction of IL-6 mRNA and protein, but not IL-1β.

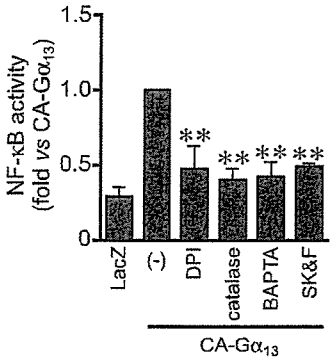

Fig. 3. Involvement of ROS and Ca^{2+} in NF-κB activation induced by $G\alpha_{13}$ activation. Cells were infected with LacZ and CA-$G\alpha_{13}$ at 100 MOI. Forty-two hours after infection, cells were treated for 6 h with 3 μM DPI, 100 U/ml catalase, 3 μM BAPTA-AM (BAPTA), or 30 μM SK&F96365 (SK&F) (n = 4 – 8). The fold increases were calculated by the values of CA-$G\alpha_{13}$-expressing cells set as 1. **$P<0.01$ *vs* CA-$G\alpha_{13}$-expressing cells.

Involvement of ROS in the induction of IL-1β and IL-6 by $G\alpha_{13}$ activation

A variety of evidence has suggested that ROS regulate NF-κB activity in mammalian cells (3). Thus, we next examined whether ROS participate in $G\alpha_{13}$-induced NF-κB activation and cytokine induction in cardiac fibroblasts. Treatment with 3 μM DPI, an inhibitor of NADPH oxidase, suppressed the induction of IL-1β mRNA and protein by CA-$G\alpha_{13}$ (Fig. 2: A and C). Although, the treatment with 3 μM DPI did not affect the CA-$G\alpha_{13}$-induced expression of IL-6 mRNA, DPI inhibited the increase in IL-6 protein by CA-$G\alpha_{13}$. Furthermore, the CA-$G\alpha_{13}$-induced NF-κB activation was also suppressed by 3 μM DPI or 100 U/ml catalase, an H_2O_2-degradating enzyme (Fig. 3). These results suggest that ROS mediate CA-$G\alpha_{13}$-induced increases in NF-κB activity and induction of IL-1β mRNA, IL-1β protein, and IL-6 protein.

Rho and Rho-kinase are not involved in IL-1β and IL-6 mRNAs induction by $G\alpha_{13}$ activation

It is generally thought that $G\alpha_{13}$-induced responses are exclusively mediated by small G protein Rho (19). However, the expression of C3 toxin at 100 MOI or treatment with 10 μM Y27632, a Rho-kinase inhibitor, did not affect the CA-$G\alpha_{13}$-induced increases in IL-1β and IL-6 mRNAs and NF-κB activation (Fig. 4). These results suggest that Rho and Rho-kinase do not participate in $G\alpha_{13}$-induced NF-κB activation and induction of IL-1β and IL-6 mRNAs.

Increased Ca^{2+} influx by $G\alpha_{13}$ activation

Our previous study has demonstrated that the expression of CA-Rho and CA-Rac promotes nuclear translocation of NFAT4 in cardiac fibroblasts (10). On the other hand, the present data indicate that $G\alpha_{13}$ induces NF-κB activation and IL-6 mRNA expression in a Ca^{2+}-dependent but Rho/Rho-kinase-independent mechanisms. As shown in Fig. 3, treatment with 30 μM SK&F96365, an inhibitor of receptor-activated non-selective cation channels (20), significantly suppressed NF-κB activation induced by CA-$G\alpha_{13}$. These results suggested that $G\alpha_{13}$ increases membrane Ca^{2+}-permeable channel activity that is not regulated by Rho and Rho-kinase. To examine whether $G\alpha_{13}$ regulates Ca^{2+} permeability in a Rho-independent manner, we determined the basal Ca^{2+} influx in CA-$G\alpha_{13}$-expressing cardiac fibroblasts. Under the basal conditions in normal Tyrode solution, $[Ca^{2+}]_i$ in CA-$G\alpha_{13}$-expressing cells was similar (about 60 – 90 nM) to that in green fluorescent protein

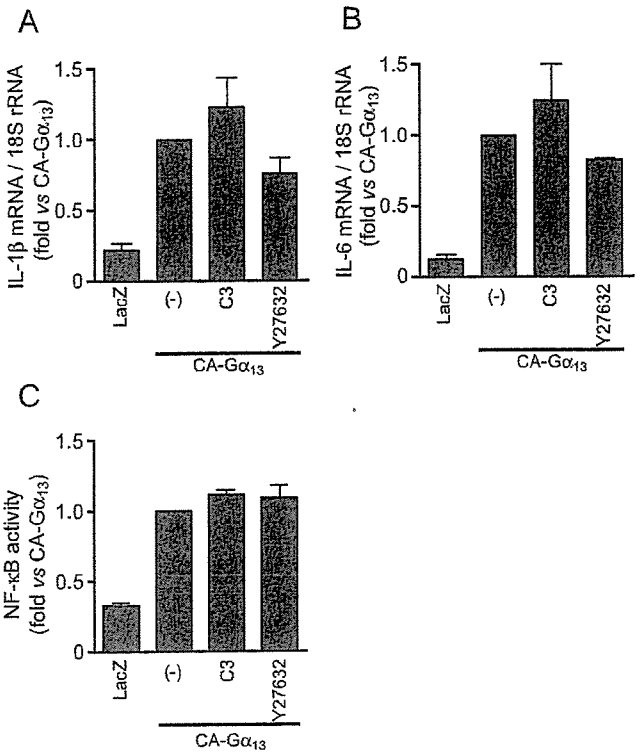

Fig. 4. Rho-and Rho-kinase-independent increases in IL-1β and IL-6 mRNAs induction by Gα_{13} activation. Cells were infected with LacZ and CA-Gα_{13} at 300 MOI or co-infected with CA-Gα_{13} at 300 MOI and C3 toxin at 100 MOI. Three hours after infection, cells were treated with 10 μM Y27632, and IL-1β (A) and IL-6 (B) mRNAs expression was determined (n = 4 – 5). C: Effects of C3 toxin and Y27632 on CA-Gα_{13}-induced NF-κB transcriptional activity were also determined. Forty-two hours after infection, cells were treated for 6 h with 10 μM Y27632, and NF-κB-dependent luciferase activity was determined (n = 4). The fold increases were calculated by the values of CA-Gα_{13}-expressing cells set as 1.

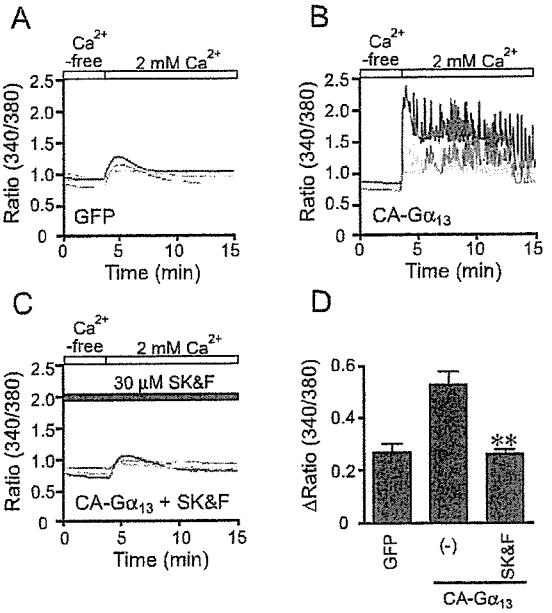

Fig. 5. Increases in basal Ca^{2+} influx induced by Gα_{13} activation. Four minutes after Ca^{2+} measurement in Ca^{2+}-free solution, basal Ca^{2+} influx was evaluated by the addition of 2 mM Ca^{2+}, and $[Ca^{2+}]_i$ was determined. SK&F96325 (SK&F, 30 μM) was treated for 10 min before the addition of extracellular Ca^{2+}. Representative time courses of Ca^{2+} responses in cardiac fibroblasts expressing GFP (A) or CA-Gα_{13} without (B) or with (C) SK&F are shown in the figure. D: The amplitude of maximum $[Ca^{2+}]_i$ rises (ΔRatio) induced by the addition of 2 mM extracellular Ca^{2+} was also calculated. $^{**}P<0.01$ *vs* CA-Gα_{13}-expressing cells.

(GFP)-expressing control cells. The resting $[Ca^{2+}]_i$ of CA-Gα_{13}-expressing cells was decreased by removal of extracellular Ca^{2+}, which was similar to the $[Ca^{2+}]_i$ level of control cells. The addition of 2 mM extracellular Ca^{2+} significantly increased $[Ca^{2+}]_i$ of CA-Gα_{13}-expressing cells (Fig. 5). This increase in $[Ca^{2+}]_i$ was completely suppressed by 30 μM SK&F96365. These results suggest that Ca^{2+} influx is constitutively increased in CA-Gα_{13}-expressing cells.

Discussion

In this study, we demonstrated that Gα_{13} activation increased the expression of IL-1β and IL-6 mRNAs and promotes the release of IL-1β and IL-6 proteins from cardiac fibroblasts (Figs. 1 and 2). It is generally thought that Gα_{12} and Gα_{13} share common signaling pathways to induce cellular responses (19). However, the induction of these cytokine mRNAs was rather specific for Gα_{13} (Fig. 1). We also found that the Gα_q signaling pathway was also involved in the expression of IL-1β mRNA in cardiac fibroblasts. Thus, our results suggest that both Gα_q and Gα_{13} regulate the expression of IL-1β mRNA, while only Gα_{13} regulates the expression of IL-6 mRNA in rat neonatal cardiac fibroblasts.

Our results also demonstrated that NF-κB was involved in the induction of both IL-1β and IL-6 mRNAs. The NF-κB activity was dependent on $[Ca^{2+}]_i$, as BAPTA-AM totally inhibited the activation (Fig. 3). However, the induction of IL-1β mRNA was not inhibited by BAPTA-AM, and the expression of IL-6 mRNA was partially inhibited by BAPTA-AM (Fig. 2: A and B). This apparent discrepancy may be explained by the several transcriptional factors involved in cytokine gene expression. The analysis of promoter regions of IL-1β and IL-6 genes shows that these regions contain several DNA binding sites for several transcriptional factors in addition to NF-κB, for instance AP-1, a ROS-sensitive transcriptional factor, and NFAT, a Ca^{2+}-sensitive transcriptional factor. These transcriptional factors synergistically regulate the transcription of cytokine mRNAs. We previously reported that CA-Gα_{13} increases NFAT and AP-1 transcriptional activities in

cardiac fibroblasts (10). Furthermore, the present results indicate that the induction of IL-1β mRNA by $G\alpha_{13}$ activation is mediated by ROS-dependent NF-κB activation, and that of IL-6 mRNA is mediated by Ca^{2+}-dependent NF-κB activation (Figs. 2 and 3). This implies that there are two kinds of NF-κB, which is functionally compartmentalized and respond separately to ROS or Ca^{2+}. We suggest that the expression of IL-1β mRNA induced by CA-$G\alpha_{13}$ requires a ROS-responsive NF-κB and AP-1 pathway, while IL-6 mRNA requires a Ca^{2+}-responsive NF-κB and NFAT pathway, even though both species of NF-κB synergistically regulate the NF-κB-dependent luciferase activity.

The amount of IL-1β released into culture medium was increased by CA-$G\alpha_{13}$, and this increase was inhibited by DPI (Fig. 2C). Thus, the inhibition of the expression of IL-1β protein by DPI was explained by the inhibition of mRNA induction. In contrast to IL-1β, the amount of IL-6 in culture medium but not the induction of IL-6 mRNA was inhibited by DPI (Fig. 2D). Therefore, DPI may inhibit the step(s) at translation and/or secretion of IL-6 protein.

As DPI suppressed $G\alpha_{13}$-induced IL-1β mRNA induction, $G\alpha_{13}$-induced ROS production may occur through NADPH oxidase activation. On the other hand, we have previously demonstrated that Rho and Rho-kinase mediate Rac-dependent NADPH oxidase activation upon Ang II receptor stimulation (10, 15). However, Rho and Rho-kinase did not participate in CA-$G\alpha_{13}$-induced NF-κB activity and cytokine mRNAs induction (Fig. 4). Thus, the Rho-independent pathway leading to NADPH oxidase activation may be activated by $G\alpha_{13}$ activation in cardiac fibroblasts.

In non-excitable cells, voltage-independent receptor-activated nonselective cation channels, including store-operated Ca^{2+} channels and transient receptor potential (TRP) channels, regulate basal Ca^{2+} influx (21). In fact, the CA-$G\alpha_{13}$-induced increases in $[Ca^{2+}]_i$ were completely suppressed by the treatment with SK&F96365. Thus, these results suggest that $G\alpha_{13}$-induced increase in Ca^{2+} influx is mediated by continuous activation of the nonselective cation channels in rat cardiac fibroblasts. This idea is in part supported by the previous report that stimulation of endothelin-1 receptor increased sustained Ca^{2+} influx through activation of G_{12} family G protein in rat arterial smooth muscle cells (20). We have previously reported that Rac1 is involved in JNK activation by regulating $[Ca^{2+}]_i$ in the H9c2 myoblast cell line (22). We have also demonstrated that $G\alpha_{13}$ activation by Ang II receptor stimulation increases Rac activity in cardiomyocytes (10, 15). However, the expression of CA-Rac1 did not affect IL-6 mRNA induction (data not shown). Therefore, another mechanism should be involved in $G\alpha_{13}$-induced activation of Ca^{2+} signaling. Further study is necessary for understanding the mechanism of sustained increase in the resting $[Ca^{2+}]_i$ induced by $G\alpha_{13}$ stimulation.

We also examined the effects of SK&F96365 on IL-1β and IL-6 mRNAs expression. However, the treatment of cells with SK&F96365 increased the basal expression of these cytokine mRNAs for yet unknown reasons (data not shown). Although SK&F96365 inhibited the further increases in these mRNAs expressions, the inhibition was partial. SK&F96365 also inhibited the increases in $[Ca^{2+}]_i$ and NF-κB activity. However, these inhibitions were not reflected by inhibition of mRNA expression. The expression of dominant negative forms of TRP channels or the suppression of TRP expression by RNAi may be necessary to demonstrate the involvement of TRP channels in IL-1β and IL-6 mRNAs expressions.

Several receptors are reported to couple to one or both members of the G_{12} family G proteins, based on direct or indirect methods of evaluating G protein activation (23). These receptors include angiotensin type 1 (AT1) receptor, endothelin-1 receptor, lysophosphatidic acid receptor, and 5-HT receptor. In the present study, we have demonstrated that $G\alpha_{13}$ activation increases the expression of IL-1β and IL-6 mRNAs and proteins in cardiac fibroblasts. As the stimulation of $5\text{-}HT_{2B}$ receptor or AT1 receptor has been reported to increase IL-1β or IL-6 production (5, 8), $G\alpha_{13}$ signaling pathways may participate in receptor-stimulated cytokine production in cardiac fibroblasts. We have not yet examined whether G_{13}-coupled receptor stimulation actually increases the expression of IL-1β and IL-6 mRNAs and proteins through the above pathways. Further studies will be necessary for the understanding of roles of $G\alpha_{13}$ signaling pathways in cytokine induction of cardiac fibroblasts.

A recent report has suggested that the strength of receptor signaling is centrally controlled through a cooperative loop between Ca^{2+} and an oxidant signal in B lymphocytes (24). We have previously demonstrated that both ROS and Ca^{2+} are required for $G_{12/13}$-mediated NFAT activation upon Ang II receptor stimulation in cardiac fibroblasts (10). Thus, ROS and Ca^{2+} generated by $G\alpha_{13}$ activation may cooperatively control the amplitude and duration of G_{13} protein-coupled receptor signaling in cardiac fibroblasts.

In conclusion, we have demonstrated a signal transduction pathway of $G\alpha_{13}$-induced increases in IL-1β and IL-6 mRNAs expression through NF-κB activation. NF-κB activation is regulated by both ROS and Ca^{2+}. However, these two signaling mediators distinctly regulate cytokine mRNA induction: ROS mediate IL-1β

mRNA induction and Ca^{2+} mediates IL-6 mRNA induction. The involvement of $G\alpha_{13}$ in cytokine mRNA induction in cardiac fibroblasts will provide a new insight into the cell-cell communication between cardiomyocytes and cardiac fibroblasts.

Acknowledgments

We thank Dr. Ryuji Inoue and Dr. Yushi Ito (Department of Pharmacology, Graduate School of Medical Sciences, Kyushu University) for the Aquacosmos imaging system, Dr. Hideki Sumimoto (Institute of Bioregulation, Kyushu University) for the luminometer, and Dr. Shigehiro Ohdo (Department of Medico-Pharmaceutical Sciences, Graduate School of Pharmaceutical Sciences, Kyushu University) for the Applied Biosystems 7500 Real-Time PCR System. We also thank Dr. Hiroyuki Tanaka (Department of Medical Plant Breeding, Graduate School of Pharmaceutical Sciences, Kyushu University) for help in the ELISA assay. This work was supported in part by a research grant (to M.N. and H.K.) from the Ministry of Education, Culture, Sports, Science, and Technology of Japan; in part by grants (to M.N.) from The Naito Foundation, The Uehara Foundation, The Kanae Foundation, The Suzuken Memorial Foundation, The Nakajima Memorial Foundation, Kao Foundation for Arts and Sciences, Takeda Science Foundation, and Japan Heart Foundation Research Grant; and a grant from Astellas Foundation for Research on Metabolic Disorders (to H. Kurose).

References

1 Brown RD, Ambler SK, Mitchell MD, Long CS. The cardiac fibroblast: therapeutic target in myocardial remodeling and failure. Annu Rev Pharmacol Toxicol. 2005;45:657–687.
2 Manabe I, Shindo T, Nagai R. Gene expression in fibroblasts and fibrosis: involvement in cardiac hypertrophy. Circ Res. 2002;91:1103–1113.
3 Siwik DA, Colucci WS. Regulation of matrix metalloproteinases by cytokines and reactive oxygen/nitrogen species in the myocardium. Heart Fail Rev. 2004;9:43–51.
4 Murray DR, Prabhu SD, Chandrasekar B. Chronic β-adrenergic stimulation induces myocardial proinflammatory cytokine expression. Circulation 2000;101:2338–2341.
5 Jaffre F, Callebert J, Sarre A, Etienne N, Nebigil CG, Launay JM, et al. Involvement of the serotonin 5-HT_{2B} receptor in cardiac hypertrophy linked to sympathetic stimulation: control of interleukin-6, interleukin-1beta, and tumor necrosis factor-alpha cytokine production by ventricular fibroblasts. Circulation. 2004;110:969–974.
6 Thaik CM, Calderone A, Takahashi N, Colucci WS. Interleukin-1β modulates the growth and phenotype of neonatal rat cardiac myocytes. J Clin Invest. 1995;96:1093–1099.
7 Fernandez L, Mosquera JA. Interleukin-1 increases fibronectin production by cultured rat cardiac fibroblasts. Pathobiology. 2002–2003;70:191–196.
8 Sano M, Fukuda K, Kodama H, Pan J, Saito M, Matsuzaki J, et al. Interleukin-6 family of cytokines mediate angiotensin II-induced cardiac hypertrophy in rodent cardiomyocytes. J Biol Chem. 2000;275:29717–29723.
9 Wollert KC, Drexler H. The role of interleukin-6 in the failing heart. Heart Fail Rev. 2001;6:95–103.
10 Fujii T, Onohara N, Maruyama Y, Tanabe S, Kobayashi H, Fukutomi M, et al. $G\alpha_{12/13}$-mediated production of reactive oxygen species is critical for angiotensin receptor-induced NFAT activation in cardiac fibroblasts. J Biol Chem. 2005;280:23041–23047.
11 Abbott KL, Loss II JR, Robida AM, Murphy TJ. Evidence that $G\alpha_q$-coupled receptor-induced interleukin-6 mRNA in vascular smooth muscle cells involves the nuclear factor of activated T cells. Mol Pharmacol. 2000;58:946–953.
12 Kurose H. $G\alpha_{12}$ and $G\alpha_{13}$ as key regulatory mediator in signal transduction. Life Sci. 2003;74:155–161.
13 Maruyama Y, Nishida M, Sugimoto Y, Tanabe S, Turner J H, Kozasa T, et al. $G\alpha_{12/13}$ mediates α_1-adrenergic receptor-induced cardiac hypertrophy. Circ Res. 2002;91:961–969.
14 Arai K, Maruyama Y, Nishida M, Tanabe S, Takagahara S, Kozasa T, et al. Differential requirement of $G\alpha_{12}$, $G\alpha_{13}$, $G\alpha_q$, and $G\beta\gamma$ for endothelin-1-induced c-Jun NH_2-terminal kinase and extracellular signal-regulated kinase activation. Mol Pharmacol. 2003;63:478–488.
15 Nishida M, Tanabe S, Maruyama Y, Mangmool S, Urayama K, Nagamatsu Y, et al. $G\alpha_{12/13}$- and reactive oxygen species-dependent activation of c-Jun NH_2-terminal kinase and p38 mitogen-activated protein kinase by angiotensin receptor stimulation in rat neonatal cardiomyocytes. J Biol Chem. 2005;280:18434–18441.
16 Nishida M, Maruyama Y, Tanaka R, Kontani K, Nagao T, Kurose H. $G\alpha_i$ and $G\alpha_o$ are target proteins of reactive oxygen species. Nature. 2000;408:492–495.
17 Monks BG, Martell BA, Buras JA, Fenton MJ. An upstream protein interacts with a distinct protein that binds to the cap site of the human interleukin 1β gene. Mol Immunol. 1994;31:139–151.
18 Kaiser P, Rothwell L, Goodchild M, Bumstead N. The chicken proinflammatory cytokines interleukin-1β and interleukin-6: differences in gene structure and genetic location compared with their mammalian orthologues. Anim Genet. 2004;35:169–175.
19 Wettschureck N, Offermanns S. Mammalian G proteins and their cell type specific functions. Physiol Rev. 2005;85:1159–1204.
20 Kawanabe Y, Okamoto Y, Miwa S, Hashimoto N, Masaki T. Molecular mechanisms for the activation of voltage-independent Ca^{2+} channels by endothelin-1 in chinese hamster ovary cells stably expressing human $endothelin_A$ receptors. Mol Pharmacol. 2002;62:75–80.
21 Clapham DE. TRP channels as cellular sensors. Nature. 2003;426:517–524.
22 Nishida M, Nagao T, Kurose H. Activation of Rac1 increases c-Jun NH_2-terminal kinase activity and DNA fragmentation in a calcium-dependent manner in rat myoblast cell line H9c2. Biochem Biophys Res Commun. 1999;262:350–354.
23 Riobo NA, Manning DR. Receptors coupled to heterotrimeric G proteins of the G_{12} family. Trends Pharmacol Sci. 2005;26:146–154.
24 Singh DK, Kumar D, Siddiqui Z, Basu SK, Kumar V, Rao KV. The strength of receptor signaling is centrally controlled through a cooperative loop between Ca^{2+} and an oxidant signal. Cell. 2005;121:281–293.

nature chemical biology

Nitric oxide activates TRP channels by cysteine S-nitrosylation

Takashi Yoshida[1–3], Ryuji Inoue[4], Takashi Morii[5], Nobuaki Takahashi[1], Shinichiro Yamamoto[1], Yuji Hara[1], Makoto Tominaga[2,3], Shunichi Shimizu[6], Yoji Sato[7] & Yasuo Mori[1]

Transient receptor potential (TRP) proteins form plasma-membrane cation channels that act as sensors for diverse cellular stimuli. Here, we report a novel activation mechanism mediated by cysteine S-nitrosylation in TRP channels. Recombinant TRPC1, TRPC4, TRPC5, TRPV1, TRPV3 and TRPV4 of the TRPC and TRPV families, which are commonly classified as receptor-activated channels and thermosensor channels, induce entry of Ca^{2+} into cells in response to nitric oxide (NO). Labeling and functional assays using cysteine mutants, together with membrane sidedness in activating reactive disulfides, show that cytoplasmically accessible Cys553 and nearby Cys558 are nitrosylation sites mediating NO sensitivity in TRPC5. The responsive TRP proteins have conserved cysteines on the same N-terminal side of the pore region. Notably, nitrosylation of native TRPC5 upon G protein–coupled ATP receptor stimulation elicits entry of Ca^{2+} into endothelial cells. These findings reveal the structural motif for the NO-sensitive activation gate in TRP channels and indicate that NO sensors are a new functional category of cellular receptors extending over different TRP families.

Ionized calcium (Ca^{2+}) is the most common signal-transduction molecule in cells ranging from bacteria to brain neurons[1]. Ca^{2+} is derived from two sources: from outside of cells, Ca^{2+} enters by passing through Ca^{2+}-permeable channels in the plasma membrane; from the inside of cells, it can be released from the endoplasmic reticulum (ER) through channels embedded in internal membrane networks. Groups of plasma membrane channels that are permeable to Ca^{2+} (or cations in general) act as sensors by translating cellular stimuli into electrical signals—namely membrane potential changes—or chemical signals such as changes in intracellular Ca^{2+} concentration ($([Ca^{2+}]_i)$[2–4]. *Drosophila melanogaster* TRP protein and its homologs are putative six-transmembrane polypeptide subunits that assemble into tetramers to form channels. In mammalian systems, TRP channels comprise six related protein subfamilies: TRPC, TRPV, TRPM, TRPA, TRPP and TRPML (ref. 5).

TRP channels are activated by diverse stimuli, including receptor stimulation, heat, osmotic pressure, and mechanical and oxidative stress from the extracellular environment and from inside the cell[3,4]. The TRPC homologs are receptor-activated Ca^{2+}-permeable cation channels (RACCs) that are activated upon receptor stimulation that induces phospholipase C (PLC) to hydrolyze phosphatidylinositol-4,5-biphosphate (PIP_2) into inositol-1,4,5-trisphosphate (IP_3) and diacylglycerol[6,7]. RACCs include store-operated channels (SOCs) activated by IP_3-induced Ca^{2+} release and depletion of ER Ca^{2+} stores. Among seven TRPC homologs (TRPC1, TRPC2, TRPC3, TRPC4, TRPC5, TRPC6 andTRPC7), TRPC1, TRPC3 and TRPC4 form SOCs, whereas TRPC5, TRPC6, TRPC7 and some TRPC3 channels are distinguishable from SOCs. In contrast to TRPCs, TRPV Ca^{2+}-permeable channels can be functionally defined as thermosensors [3,5,8,9]. TRPV1, which was originally identified as the receptor for the vanilloid compound capsaicin, is responsive to heat (>43 °C), to proton concentration (pH < 5.6), to the intrinsic ligand anandamide and to PLC-linked receptor stimulation[5]. High temperature also activates TRPV2 (>52 °C), TRPV3 (>31 °C or >39 °C) and TRPV4 (>27 °C). TRPV5 and TRPV6 comprise a different subfamily because they are activated by $[Ca^{2+}]_i$ (refs. 3,5). Thus, characteristic activation triggers functionally distinguish sensor cation channels formed by molecularly distinct TRPC- and TRPV-family proteins.

NO is another pleiotropic cell signaling molecule that controls diverse biological processes[10,11]. According to the classical view, cyclic GMP is the mediator of NO signaling. However, the importance of a cGMP-independent pathway through protein S-nitrosylation is increasingly recognized by researchers in the field of NO signal transduction[10,11]. Because nitrosothiols are exceptionally labile owing to their reactivity with intracellular reducing reagents such as ascorbic acid, S-nitrosylation functions as a reversible post-translational modification analogous to phosphorylation. Cysteine modifications of proteins are also elicited by other NO-related species, reactive oxygen species, glutathione disulfide and free sulfhydryl-specific reactive disulfide[11,12]. However, these modifications are rather

[1]Department of Synthetic Chemistry and Biological Chemistry, Graduate School of Engineering, Kyoto University, Kyoto 615-8510, Japan. [2]Center for Integrative Bioscience, National Institute for Physiological Sciences, Okazaki, Aichi 444-8585, Japan. [3]School of Life Science, The Graduate University for Advanced Studies, Okazaki, Aichi 444-8585, Japan. [4]Department of Physiology, Fukuoka University, Fukuoka 814-0180, Japan. [5]Institute of Advanced Energy, Kyoto University, Uji, Kyoto 611-0011, Japan. [6]Department of Pathophysiology, School of Pharmaceutical Sciences, Showa University, Tokyo 142-8555, Japan. [7]Division of Cellular and Gene Therapy Products, National Institute of Health Sciences, Tokyo 158-8510, Japan. Correspondence should be addressed to Y.M. (mori@sbchem.kyoto-u.ac.jp).

Received 20 March; accepted 4 August; published online 24 September 2006; doi:10.1038/nchembio821

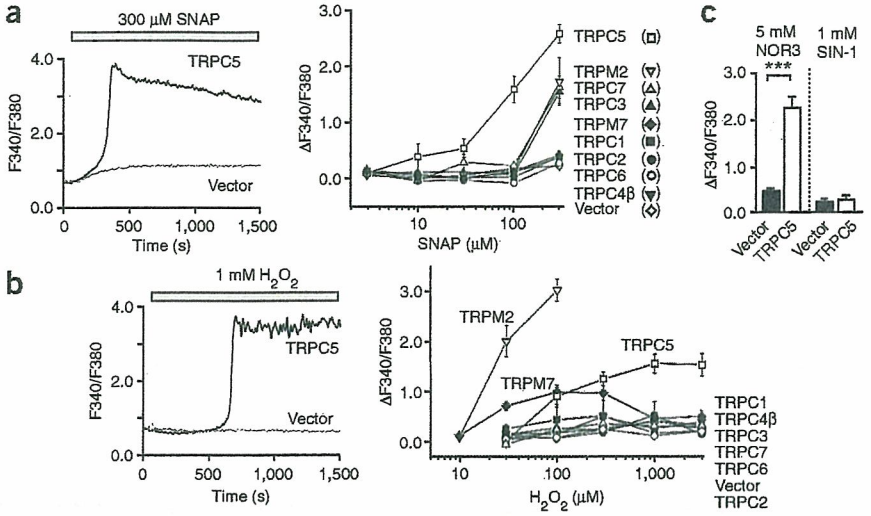

Figure 1 NO activates TRPC5-mediated Ca^{2+} response. (**a**,**b**) $[Ca^{2+}]_i$ rises (340:380-nm fluorescence ratio; F340/F380) evoked by SNAP (**a**) and H_2O_2 (**b**) applied during periods indicated by shaded bars in the presence of 2 mM extracellular Ca^{2+}. Representative time courses (left) and dose-response relationships of maximal $[Ca^{2+}]_i$ rises (ΔF340/F380) (right) in HEK cells transfected with TRP homologs or vector (n = 6–61). Data points are mean ± s.e.m. (**c**) Maximal $[Ca^{2+}]_i$ rises induced by NOR3 and SIN-1 (n = 19–31). ***$P < 0.001$.

pathophysiological, although they can be viewed as existing on a continuum that relates concentrations of reactive species to the form and consequences of modification. Thus, S-nitrosylation alone conveys physiological redox-based cellular signals[11].

Ca^{2+} and NO signals are precisely coordinated with each other. Among three distinct isoforms of NO synthases (NOSs) responsible for NO production, $[Ca^{2+}]_i$ elevation is essential for activation of Ca^{2+}-dependent endothelial NOS (eNOS) and neuronal NOS (nNOS)[13]. Furthermore, IP_3-induced Ca^{2+} release and RACC-mediated Ca^{2+} influx via PLC activation is efficiently evoked upon receptor stimulation by physiological agonists such as vasodilators, thereby leading to eNOS activation in endothelial cells and other cell types[14–16]. However, it is still unclear whether activation of eNOS requires specific modes of upstream Ca^{2+}-mobilizing mechanism or RACC subtypes formed by particular TRPCs (refs. 16–20), whereas NMDA (*N*-methyl-D-aspartate) receptors in neurons and L-type voltage-dependent Ca^{2+} channels in muscles are known to conduct nNOS-activating Ca^{2+} influx[21]. Feedback regulation of Ca^{2+} signaling by NO remains even more elusive[22]: both positive[23–25] and negative[26,27] regulation by NO of Ca^{2+} mobilization pathways including RACCs has been reported. Physiological protein targets for cysteine S-nitrosylation include postsynaptic NMDA receptors and skeletal-muscle ryanodine-receptor Ca^{2+} release channels[11]. However, these channels involved in Ca^{2+} signaling are very restricted in tissue distribution and have specific physiological functions, compared with the widely recognized generality of NO signaling via protein S-nitrosylation, Ca^{2+} signaling, and their cross talk. Therefore, to understand more general molecular mechanisms that link the two key signals, S-nitrosylation targets must be identified among more ubiquitous Ca^{2+}-mobilizing ion channels. This would ultimately provide insights into the activation gating that underlies sensor function in TRP channels.

Here, we describe cysteine modification as a previously unknown mechanism that triggers activation gating of TRP channels. Chemical labeling assays using TRPC5 mutants reveal modification of Cys553 and Cys558 (whose counterparts are harbored by the NO-responsive TRPC and TRPV members) on the N-terminal side of the pore-forming region. Further studies using cultured endothelial cells, in combination with the previously reported wide distribution of the NO-responsive TRPC and TRPV channels among diverse tissues[5],

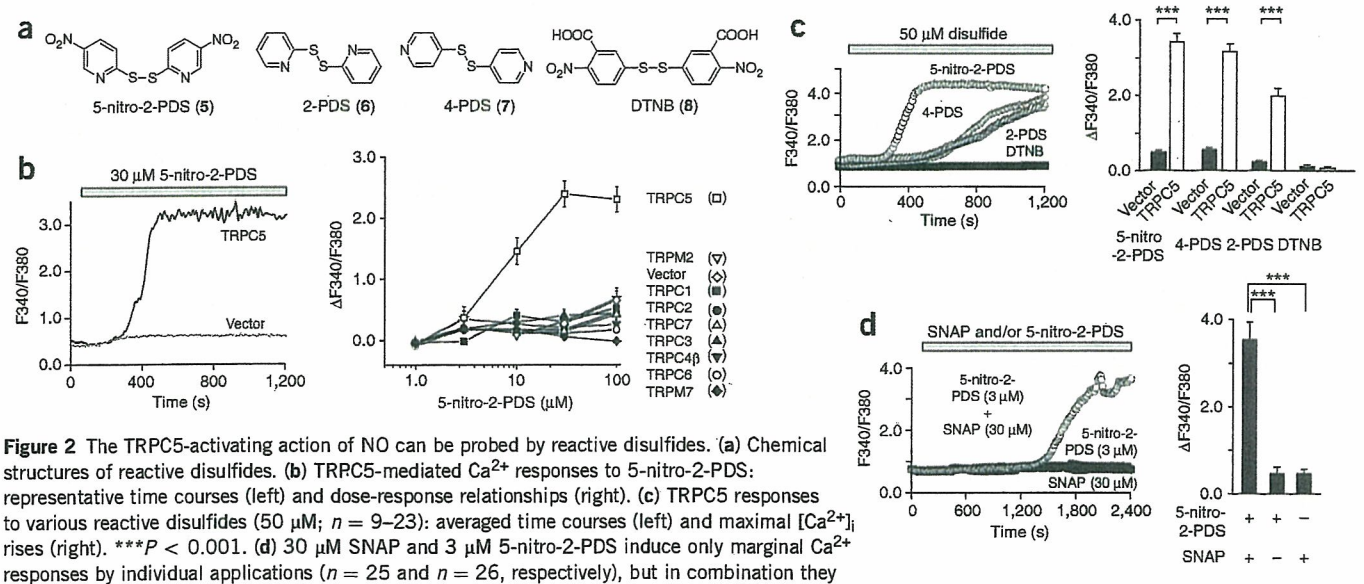

Figure 2 The TRPC5-activating action of NO can be probed by reactive disulfides. (**a**) Chemical structures of reactive disulfides. (**b**) TRPC5-mediated Ca^{2+} responses to 5-nitro-2-PDS: representative time courses (left) and dose-response relationships (right). (**c**) TRPC5 responses to various reactive disulfides (50 μM; n = 9–23): averaged time courses (left) and maximal $[Ca^{2+}]_i$ rises (right). ***$P < 0.001$. (**d**) 30 μM SNAP and 3 μM 5-nitro-2-PDS induce only marginal Ca^{2+} responses by individual applications (n = 25 and n = 26, respectively), but in combination they trigger robust TRPC5-mediated Ca^{2+} responses (n = 18): averaged time courses (left) and maximal $[Ca^{2+}]_i$ rises (right). Data points are mean ± s.e.m. ***$P < 0.001$.

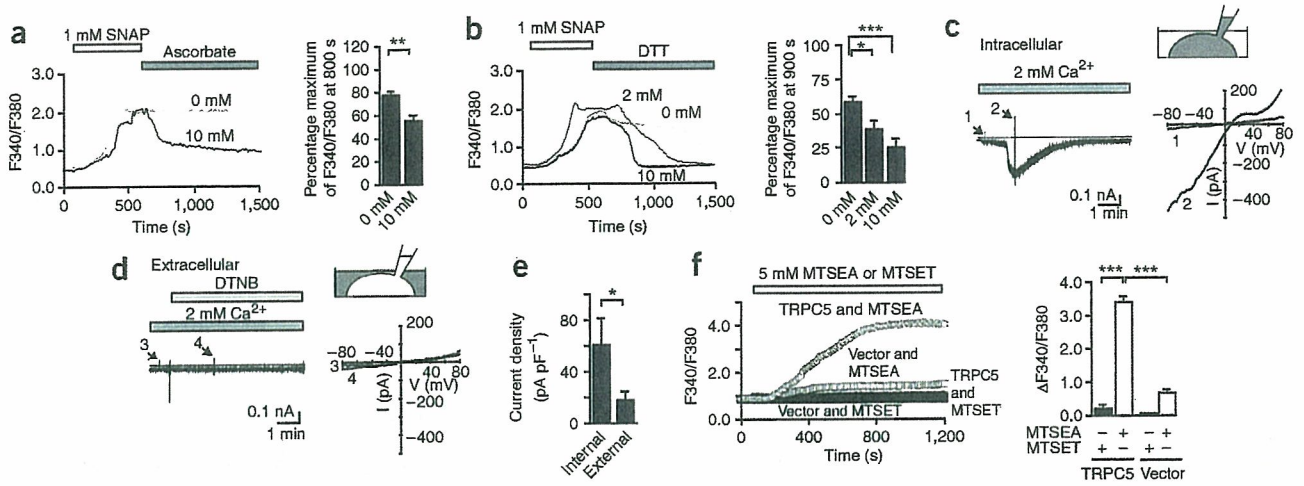

Figure 3 Chemical characterization and membrane sidedness of the action of NO and reactive disulfide in activating TRPC5 channels. (**a**,**b**) Ascorbate and DTT suppress TRPC5 responses to SNAP: representative time courses (left) and percentages of $[Ca^{2+}]_i$ rises (right) at 800 s (**a**) and 900 s (**b**) relative to maximal rises (n = 17–42). $^*P < 0.05$, $^{**}P < 0.01$ and $^{***}P < 0.001$. (**c**,**d**) Whole-cell TRPC5 currents are activated by DTNB (left) via internal dialysis (10 μM) (**c**) but not via external application (30 μM) (**d**). I–V relations were determined using 50-ms positive-voltage ramps from –80 mV to +80 mV applied at time points indicated as 1–4 (right). (**e**) Peak current densities (n = 22–27). $^*P < 0.05$. (**f**) Ca^{2+} responses to MTSEA or MTSET: average time courses (left) and maximal $[Ca^{2+}]_i$ rises (right) (n = 17–33). Data points are mean ± s.e.m. $^{***}P < 0.001$.

suggest that the group of native S-nitrosylation–sensitive TRP channels mediates a ubiquitous mechanism that is critical for feedback regulation of Ca^{2+} signals by NO.

RESULTS

NO activates TRPC5 channels via sulfhydryl modifications

Recombinant expression of TRPC5 elicited robust elevation of $[Ca^{2+}]_i$ in response to the NO donor *S*-nitroso-*N*-acetyl-DL-penicillamine (SNAP, **1**) in human embryonic kidney (HEK) cells (**Fig. 1**). A similar $[Ca^{2+}]_i$ increase was induced by another NO donor, (±)-(*E*)-4-ethyl-2-[(*E*)-hydroxyimino]-5-nitro-3-hexenamide (NOR3, **2**), but not by the peroxynitrite donor 3-(4-morpholinyl)sydnonimine hydrochloride (SIN-1, **3**) (**Fig. 1c**). The SNAP-induced Ca^{2+} response is attributable mainly to Ca^{2+} entry through the TRPC5 channel, as SNAP evoked only marginal $[Ca^{2+}]_i$ rises in TRPC5-expressing cells after omission of extracellular Ca^{2+} (**Supplementary Fig. 1** online) and in vector-transfected control cells (**Fig. 1a**). The sensitivity of TRPC5 to SNAP was prominent among TRPC homologs: substantial $[Ca^{2+}]_i$ rises distinguishable from the control were elicited by TRPC5 in response to SNAP at 10 μM, but such rises were elicited by TRPC3 and TRPC7 and by the redox status–sensitive Ca^{2+}-permeable cation channel TRPM2 (ref. 28) only at much higher concentrations of SNAP, such as 300 μM. TRPM2 mediated pronounced Ca^{2+} responses to H_2O_2 (**Fig. 1b**). TRPC5 was the only TRPC homolog that elicited robust Ca^{2+} responses to H_2O_2 at 100 μM (**Fig. 1b**). Furthermore, ATP/Mg^{2+}-sensitive Ca^{2+}-permeable cation channel TRPM7 (ref. 3), which responds to oxygen- and glucose-deprived conditions[29], was responsive to H_2O_2 but not to SNAP (**Fig. 1a**,**b**). Thus, prominent sensitivity to NO is characteristic of TRPC5 channels.

NO-induced Ca^{2+} responses mediated by TRPC5 were resistant to the guanylate cyclase inhibitor 1H-[1,2,4]oxadiazolo[4,3-a]quinoxalin-1-one (ODQ, **4**) (**Supplementary Fig. 1**). This suggests that NO acts through cGMP-independent pathways such as nitrosylation of free sulfhydryl groups of cysteine residues. Indeed, among reactive disulfides that selectively detect free sulfhydryl groups of cysteine residues in proteins (**Fig. 2a**), membrane-permeable pyridyldisulfides (PDS) such as 2,2′-dithiobis(5-nitropyridine) (5-nitro-2-PDS, **5**), 2,2′-dithiodipyridine (2-PDS, **6**) and 4,4′-dithiodipyridine (4-PDS, **7**) induced robust $[Ca^{2+}]_i$ rises in cells expressing TRPC5, whereas membrane-impermeable analog 5,5′-dithiobis(2-nitrobenzoic acid) (DTNB, **8**) elicited marginal $[Ca^{2+}]_i$ elevation that was indistinguishable from the control (**Fig. 2b**,**c**). Expression of other TRPCs and of TRPM2 and TRPM7 failed to elicit 5-nitro-2-PDS–induced $[Ca^{2+}]_i$ increases that significantly surpassed the control. TRPC5 responses to SNAP, 5-nitro-2-PDS and H_2O_2 were preceded by time lags after application (time to half peak was 305 ± 14.4 s for 300 μM SNAP (n = 52), 780 ± 50.1 s for 1 mM H_2O_2 (n = 18), and 425 ± 32.7 s for 30 μM 5-nitro-2-PDS (n = 17)). Robust TRPC5-mediated responses were evoked by simultaneous application of SNAP (30 μM) and 5-nitro-2-PDS (3 μM), which both induced slight TRPC5 responses when individually applied (**Fig. 2d**). Furthermore, maximal responses elicited by 1 mM SNAP were not potentiated by the addition of 30 μM 5-nitro-2-PDS, and vice versa (**Supplementary Fig. 2** online). These relationships may imply a common action site (or sites) for NO and 5-nitro-2-PDS in inducing TRPC5 responses. Thus, reactive disulfides are useful tools for identifying the free sulfhydryl targets of NO in TRPC5 activation.

The reducing agent ascorbate (**9**) significantly (P = 0.008) diminished SNAP-induced TRPC5 responses (**Fig. 3a**) but not 5-nitro-2-PDS–induced TRPC5 responses (**Supplementary Fig. 2**). Dithiothreitol (DTT, **10**) had a potent suppressive effect on both responses (**Fig. 3b** and **Supplementary Fig. 2**). Considering the reported selective reduction of nitrosothiol by ascorbate to reform thiol[10], this result supports the notion that NO and reactive disulfides form nitrosothiols and disulfide bonds, respectively, on cysteine residues in eliciting TRPC5-mediated responses. After washout, the TRPC5 response to SNAP was slowly attenuated (**Fig. 3a**,**b**), in contrast to the sustained TRPC5 response to 5-nitro-2-PDS (**Supplementary Fig. 2**). This suggests that the nitrosylation is reversed by intrinsic antioxidants in HEK cells. The modification stability, the TRPC5 selectivity and the substitutability for NO of reactive disulfides prompted us to use them as tools in the following studies on TRPC5 activation.

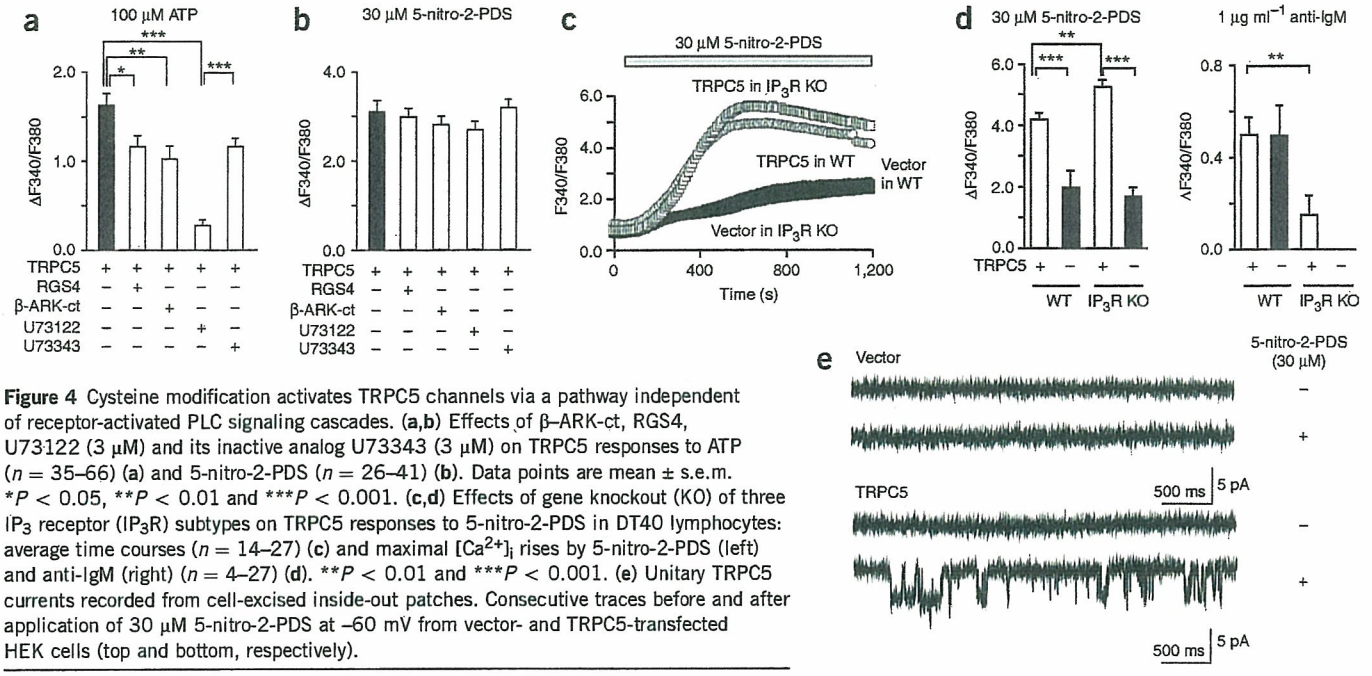

Figure 4 Cysteine modification activates TRPC5 channels via a pathway independent of receptor-activated PLC signaling cascades. (**a**,**b**) Effects of β-ARK-ct, RGS4, U73122 (3 μM) and its inactive analog U73343 (3 μM) on TRPC5 responses to ATP (n = 35–66) (**a**) and 5-nitro-2-PDS (n = 26–41) (**b**). Data points are mean ± s.e.m. $^*P < 0.05$, $^{**}P < 0.01$ and $^{***}P < 0.001$. (**c**,**d**) Effects of gene knockout (KO) of three IP_3 receptor (IP_3R) subtypes on TRPC5 responses to 5-nitro-2-PDS in DT40 lymphocytes: average time courses (n = 14–27) (**c**) and maximal $[Ca^{2+}]_i$ rises by 5-nitro-2-PDS (left) and anti-IgM (right) (n = 4–27) (**d**). $^{**}P < 0.01$ and $^{***}P < 0.001$. (**e**) Unitary TRPC5 currents recorded from cell-excised inside-out patches. Consecutive traces before and after application of 30 μM 5-nitro-2-PDS at –60 mV from vector- and TRPC5-transfected HEK cells (top and bottom, respectively).

In TRPC5-expressing cells, 5-nitro-2-PDS–induced Ca^{2+} responses are due to Ca^{2+} entry through the TRPC5 channel, as $[Ca^{2+}]_i$ elevation was evoked predominantly upon readdition of extracellular Ca^{2+} (**Supplementary Fig. 2**). The whole-cell mode of the patch clamp method demonstrated 5-nitro-2-PDS–induced inward currents that developed gradually in TRPC5-expressing cells (n = 6), but not in control cells (n = 4), at a holding potential (V_H) of –60 mV (**Supplementary Fig. 2**). Current–voltage (I–V) relationships of the 5-nitro-2-PDS–activated currents corresponded well with previously reported receptor-activated TRPC5 currents[30]. 5-nitro-2-PDS–activated TRPC5 currents showed a resistance to washout that was slowly reversed by DTT (n = 5), which supports $[Ca^{2+}]_i$ measurements.

Membrane sidedness of modification in TRPC5 activation

The ineffectiveness of extracellular application of the membrane-impermeable DTNB (**Fig. 2c**) suggests an agonistic modification site (or sites) that is accessible only from the cytoplasmic side. We explicitly evaluated this hypothesis using the patch clamp method. Intracellular perfusion of DTNB from the patch pipette elicited TRPC5 currents at a V_H of –60 mV with a time lag of 1 to 2 min after the whole-cell mode was established (**Fig. 3c**). The I–V relationship was similar to that activated by 5-nitro-2-PDS (see above). However, extracellular DTNB exerted no significant effects on current levels or I–V relationships in TRPC5-expressing cells (**Fig. 3d**,**e**). The action of methanethiosulfonate derivatives, which directly modify free cysteine thiols by forming a disulfide bond[31], resembled the action of reactive disulfides in sidedness: membrane-permeable 2-aminoethylmethanethiosulfonate hydrobromide (MTSEA, **11**) but not membrane-impermeable [2-(trimethylammonium)ethyl]methanethiosulfonate bromide (MTSET, **12**) induced TRPC5 responses via extracellular administration (**Fig. 3f**). These results support the cytoplasmic accessibility of the site for cysteine modifications.

Identification of the site of cysteine modification in TRPC5

We have previously demonstrated metabotropic ATP receptor subtype P2Y-mediated activation of TRPC5 channels via the G-protein isoform Gq and PLC-β in HEK cells[30]. Therefore, we examined the possibility that the P2Y-activated signaling cascade has an action site (or sites) for reactive disulfides in TRPC5 activation. The quenching of G protein βγ complexes by the regulator of G-protein signaling 4 (RGS4) (P = 0.011) and the C terminus of β-adrenergic receptor kinase (β-ARK-ct) (P = 0.002), as well as the inhibition of PLC-β by the PLC inhibitor U73122 ($P < 0.001$), significantly attenuated TRPC5 responses to P2Y stimulation but failed to affect TRPC5 responses evoked by 5-nitro-2-PDS (**Fig. 4a**,**b**). Furthermore, disruption of the three IP_3 receptor subtype genes[32], which suppressed IgM-induced TRPC5 responses via B-cell receptors, significantly promoted 5-nitro-2-PDS–evoked TRPC5 responses in DT40 B lymphocytes (**Fig. 4c**,**d**). These results suggest that reactive disulfides activate the TRPC5 channel independently of P2Y-activated signals.

We examined whether reactive disulfides directly act on TRPC5 channels using the cell-excised, inside-out mode of patch clamp recording. Single-channel currents with a unitary conductance of 44.1 pS were induced in TRPC5-expressing cells (but not in control cells) by applying 5-nitro-2-PDS to the cytoplasmic side of excised patches (**Fig. 4e**). On the basis of this result, we hypothesized that the action site is localized at the plasma membrane and its associated cellular components in TRPC5-expressing cells. Therefore, we investigated the incorporation of reactive disulfides into TRPC5 channel complexes using DTNB-2Bio (**13**), a DTNB derivative that has two biotin groups attached (**Fig. 5a**; **Supplementary Scheme 1** and **Supplementary Fig. 3** online). In cells expressing green fluorescent protein (GFP)-tagged TRPC5, we incorporated DTNB-2Bio into a ~130 kDa protein band, which yielded an adduct whose molecular weight corresponds well with the calculated molecular weight of TRPC5-GFP (139 kDa) (**Fig. 5b**). Simultaneous application of SNAP inhibited the incorporation of DTNB-2Bio (**Fig. 5c**), which is consistent with the observation in the $[Ca^{2+}]_i$ measurements (**Fig. 2d**). Thus, NO and reactive disulfides share a covalent modification site in TRPC5-channel protein complexes.

Free cysteine sulfhydryls are nitrosylated by NO (refs. 11,33) and are modified by reactive disulfides via disulfide exchange reactions in

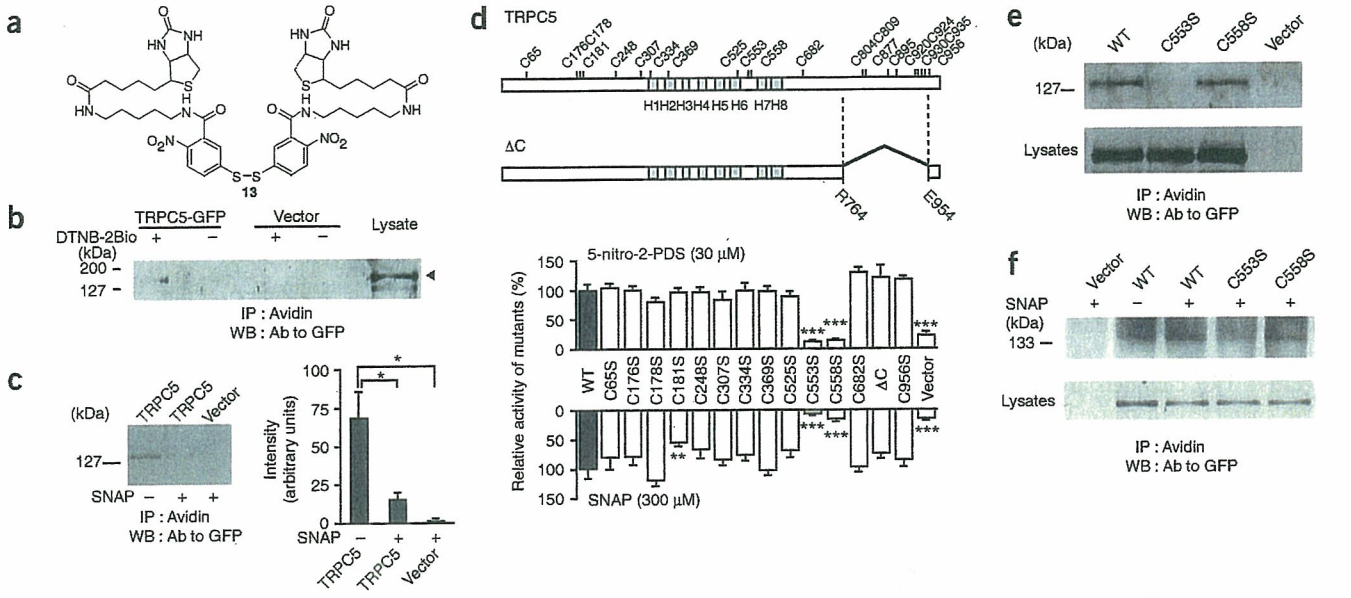

Figure 5 S-nitrosylation in TRPC5 channel protein complexes. (**a–c**) NO and reactive disulfides share incorporation site. (**a**) Chemical structure of DTNB-2Bio. (**b**) Detection of TRPC5-GFP among proteins incorporating DTNB-2Bio (100 μM) by western blot analysis (WB) using antibody to GFP. (**c**) Suppression of DTNB-2Bio incorporation by 5 mM SNAP (left); the total band intensity (right). Data points are mean ± s.e.m. $*P < 0.05$. (**d**) Cysteine residues mapped on TRPC5 (top); cysteines were replaced with serine, or deleted in the ΔC mutant (in which Arg764 through Glu954 is deleted). Relative responses to 5-nitro-2-PDS ($n = 15–48$) and to SNAP ($n = 14–31$) of TRPC5 mutants in HEK cells (bottom). $**P < 0.01$, $***P < 0.001$, compared to WT. (**e**) Effects of mutations C553S and C558S on DTNB-2Bio incorporation. WB of total cell lysates indicates comparable TRPC5 expression (lysates). (**f**) Cysteine S-nitrosylation of WT TRPC5-GFP and mutants C553S and C558S with and without SNAP treatment. IP, immunoprecipitation.

proteins[12]. Therefore, cysteine residues are the most likely modification-site candidate. We subjected every cysteine residue in TRPC5 to replacement with serine or to deletion, and then we tested the mutants for their responses to 5-nitro-2-PDS and NO (**Fig. 5d**). Mutations C553S and C558S abrogated TRPC5 responses to NO (5%, 16% and 16% of wild-type (WT) response for C553S, C558S and vector, respectively) and TRPC5 responses to 5-nitro-2-PDS (13%, 15% and 24% of WT for C553S, C558S and vector, respectively). The resistance of the mutants is not attributable to localization defects, as the mutants showed intact plasma-membrane expression (like the WT protein) in assays using the biotinylation labeling method and in observations using an evanescent wave microscope that illuminates only the subcellular area from the surface to a depth of less than 100 nm by total internal reflection (**Supplementary Fig. 4** online). TRPC5 responses to receptor stimulations were only partially suppressed by C553S and C558S mutants (**Supplementary Fig. 4**), in contrast to TRPC5 responses to NO. The DTNB-2Bio incorporation was also abolished by C553S, whereas it was unaffected by C558S (**Fig. 5e**). Cysteine S-nitrosylation detected after selective conversion into biotinylated cysteines[10] was substantially enhanced by SNAP in WT proteins (184% ± 45% of basal level). TRPC5 nitrosylation was significantly suppressed by C553S (38% ± 21% of WT with SNAP) but was suppressed less extensively by C558S (75% ± 9.7% of WT with SNAP) (**Fig. 5f**). These results indicate that Cys553 is a main nitrosylation site and a predominant modification site for reactive disulfides.

TRP channels with conserved cysteines are responsive to NO

We tested NO-sensitive channel activation for generality in the TRP superfamily (**Fig. 6**). Notably, the alignment of amino acid sequences surrounding Cys553 and Cys558 of TRPC5 with counterpart sequences shows that TRPC5's closest relatives, TRPC1 and TRPC4, as well as thermosensor channels TRPV1, TRPV3 and TRPV4, have cysteines conserved on the N-terminal side of the putative pore-forming region H7 in the linker region located between the fifth and sixth transmembrane domains S5 and S6 (the S5-S6 linker) (**Fig. 6a**)[30,34]. TRPC1, TRPC4 and TRPV1 contain two cysteines separated by four residues (like TRPC5), whereas TRPV3 and TRPV4 have two and four cysteines, respectively, in sequences distantly related to TRPC5. These cysteines predict the NO responsiveness of these TRPC and TRPV channels to cysteine modifications.

We tested the recombinants of the above TRP protein homologs for susceptibility to SNAP, 5-nitro-2-PDS and H_2O_2 in HEK cells (**Fig. 6c–h**). As shown in **Figure 1**, the differences in maximal $[Ca^{2+}]_i$ rises (ΔF340/F380) statistically tested between control cells and the total populations of cells expressing TRPC1 or TRPC4β (a splice isoform of TRPC4) alone were not significant. However, in response to SNAP (300 μM) and 5-nitro-2-PDS (30 μM), a larger fraction (7%–9%) of expressing cells showed ΔF340/F380 > 0.5 relative to control cells (2%–5%). Cells co-expressing TRPC4β and TRPC5 showed SNAP and 5-nitro-2-PDS responses comparable to those in cells expressing TRPC5 alone (**Fig. 6c,d**), whereas cells co-expressing TRPC1 and TRPC5 showed slightly suppressed (yet robust) responses (**Fig. 6f,g**). In cells co-expressing TRPC5 and TRPC4β (**Fig. 6e**) or TRPC1 (**Fig. 6h**), H_2O_2 (1 mM) evoked significantly (TRPC1; $P = 0.003$; TRPC4, $P = 0.001$) impaired responses. We immunoprecipitated TRPC5 with co-expressed TRPC1 or TRPC4β (**Fig. 6b**) and the results suggest that heteromultimeric TRPC5/TRPC1 and TRPC5/TRPC4β channels have intact NO sensitivity and H_2O_2 resistance, whereas homomultimetric TRPC5 is sensitive to both NO and H_2O_2.

We also observed activation by NO for thermosensor channels TRPV1, TRPV3 and TRPV4, as predicted (**Fig. 7**). The augmentation of $[Ca^{2+}]_i$ rises by extracellular Ca^{2+} revealed NO- and 5-nitro-2-PDS–activated Ca^{2+} entry via TRPV1, TRPV3 and TRPV4

(**Fig. 7a,b,d,e**). TRPV1 and TRPV4 were responsive to H_2O_2, but TRPV3 was relatively resistant, much like the heteromultimeric TRPC channels (**Fig. 6e,h** and **Fig. 7c,f**). The TRPV1 mutant having substitutions at Cys616 and Cys621 (V1 mut) showed significantly (P = 0.005–0.031) suppressed responses to NO and other agents (**Fig. 7d–f**), and to nitrosylation (**Fig. 7g**). Notably, the H^+ sensitivity and heat sensitivity of TRPV1 was enhanced by NO (**Fig. 7h,i**). This enhancement was abolished by the mutation, whereas H^+ and heat responses without SNAP application (**Fig. 7h,i**) and surface expression (**Supplementary Fig. 4**) of the mutant were intact. Thus, channel activation regulated by nitrosylation is conserved among several TRP proteins.

Native TRP channels are activated by NO in endothelial cells

We characterized native Ca^{2+} influx triggered in response to NO in vascular endothelial cells (**Figs. 8** and **9**). As reported[20,35], cultured bovine aortic endothelial cells (BAEC) showed substantial enhancements of TRPC5 protein expression (**Fig. 8a**) and Ca^{2+} responses after 3 d of culture (**Supplementary Fig. 5** online). To resolve involvements of TRPC5 in native Ca^{2+} influx, we measured $[Ca^{2+}]_i$ rises upon readdition of extracellular Ca^{2+} under agent stimulation after introducing TRPC5-selective small interference RNA (siTRPC5) and the dominant negative construct of TRPC5 (TRPC5-DN)[36] in BAEC. Ca^{2+} influx evoked by NO and 5-nitro-2-PDS was significantly suppressed by siTRPC5 and TRPC5-DN in BAEC (**Fig. 9a,b**). In contrast, H_2O_2 induced only marginal Ca^{2+} influx that was insensitive to siTRPC5 and TRPC5-DN (**Fig. 9c**). This activator sensitivity is similar to that observed in recombinant TRPC5/TRPC1 and TRPC5/TRPC4β heteromultimers in HEK cells (**Fig. 6c–h**) and is consistent with confocal immunoimages showing superimposable distribution of TRPC5 with TRPC1 and TRPC4 at the plasma membrane area

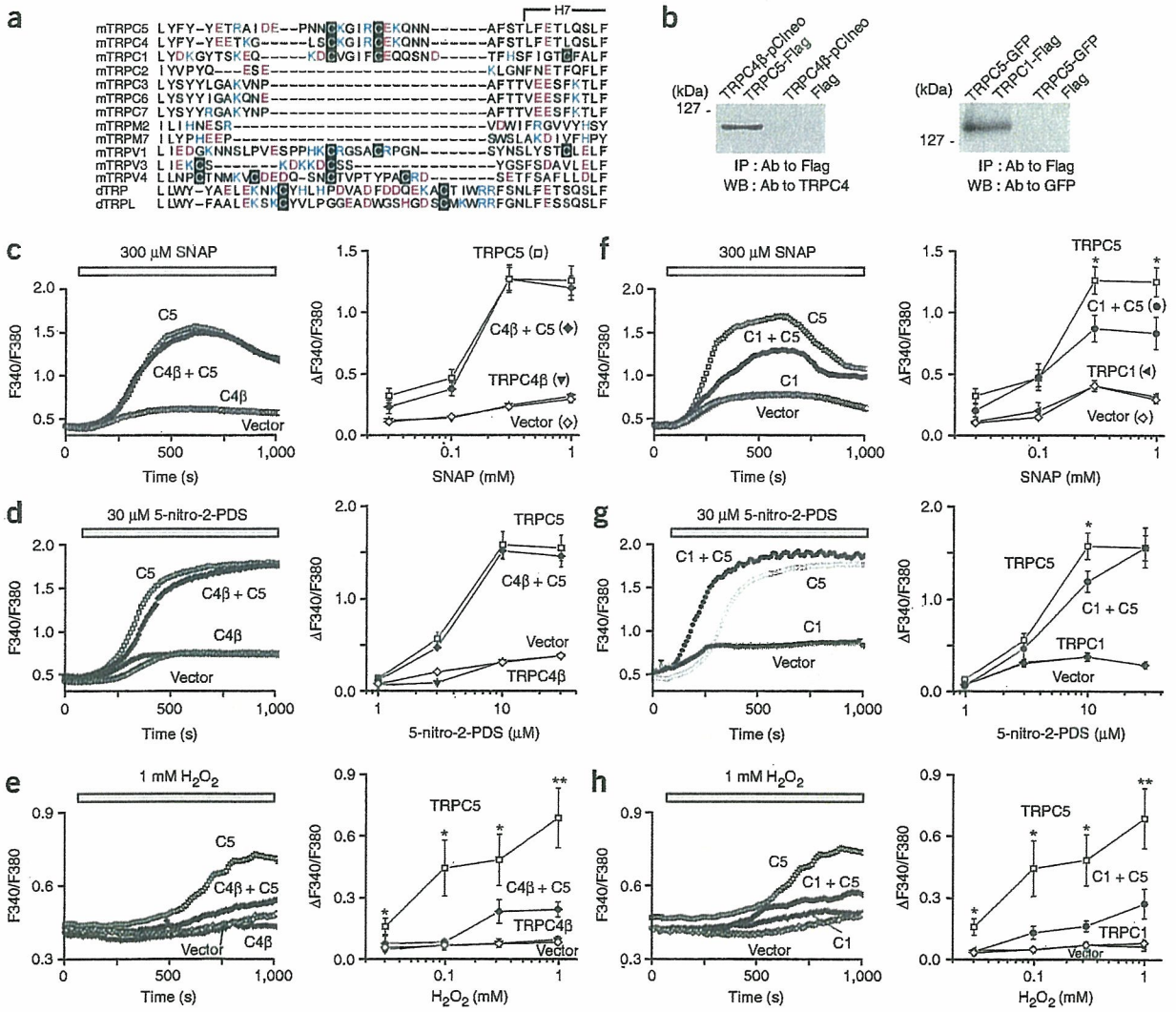

Figure 6 Molecular conservation of NO-induced activation in TRP channels. (**a**) Conserved cysteine residues on the N-terminal side of putative pore-forming regions in mouse TRPC1, TRPC2, TRPC3, TRPC4, TRPC5, TRPC6, TRPC7, TRPM2, TRPM7, TRPV1, TRPV3 and TRPV4 and *D. melanogaster* TRP and TRPL. (**b**) Co-immunoprecipitation of TRPC5 with TRPC4β (top) and TRPC1 (bottom). Immunoprecipitates (IP) with antibody to Flag from HEK cells expressing TRPC4β/TRPC5-Flag or TRPC1-Flag/TRPC5-GFP were subjected to WB with antibody to TRPC4 or GFP, respectively. pCIneo is the mammalian expression plasmid. (**c–h**) Ca^{2+} responses mediated by TRPC4β/TRPC5 (**c–e**) and TRPC1/TRPC5 heteromultimers (**f–h**) in HEK cells: average time courses of responses to SNAP (**c,f**), 5-nitro-2-PDS (**d,g**) and H_2O_2 (**e,h**) (left) and dose-response relationships (n = 21–49) (right). Data points are mean ± s.e.m. $^*P < 0.05$ and $^{**}P \leq 0.01$ for TRPC5, compared to TRPC5/TRPC4 or TRPC5/TRPC1.

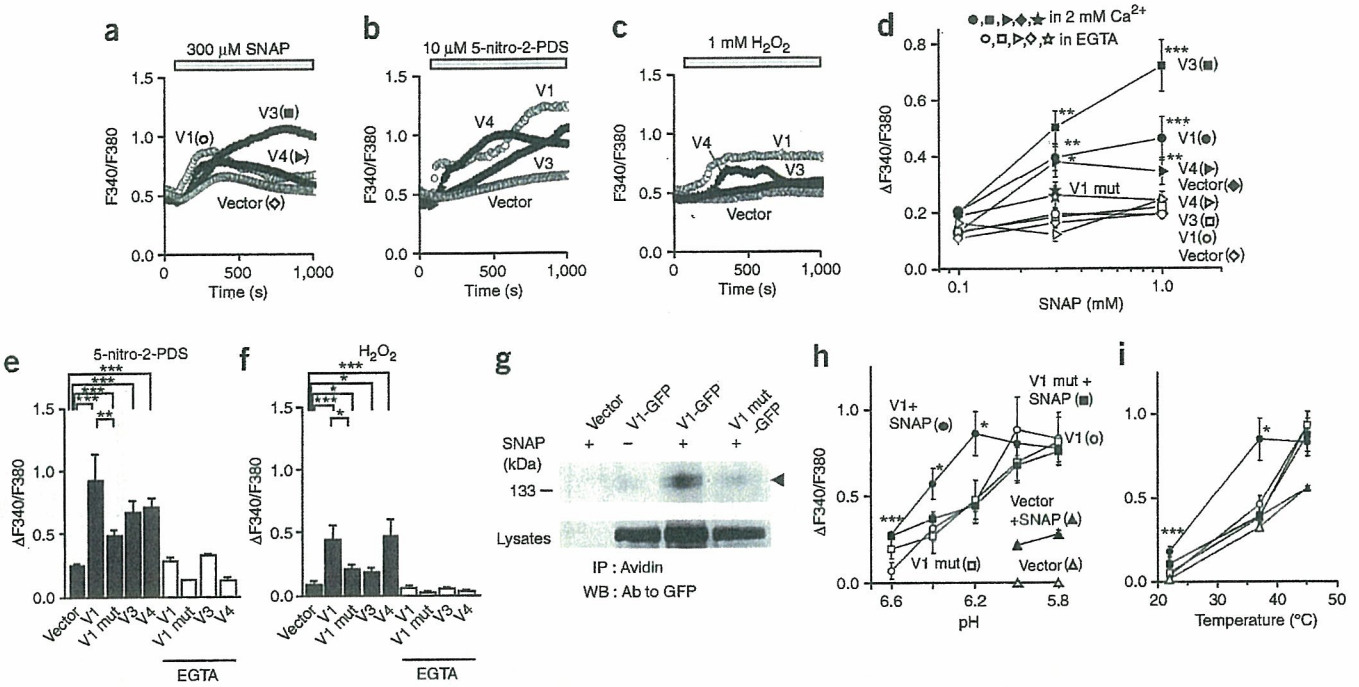

Figure 7 Regulation of TRPV channel activation by nitrosylation. (**a–f**) Ca^{2+} responses to SNAP (**a**), 5-nitro-2PDS (**b**) and H_2O_2 (**c**) mediated by rat TRPV1 and its cysteine substitution C616W C621S mutant (V1 mut), and human TRPV3 and TRPV4: average time courses (**a–c**), SNAP dose-response relationships (**d**), and maximal $[Ca^{2+}]_i$ rises by 5-nitro-2-PDS (**e**) and H_2O_2 (**f**) in the presence and absence (EGTA) of 2 mM external Ca^{2+} (n = 12–122). Data points are mean ± s.e.m. $^*P < 0.05$, $^{**}P < 0.01$ and $^{***}P < 0.001$ compared to control (vector). (**g**) S-nitrosylation of TRPV1-GFP and the mutant. (**h,i**) NO enhances H^+ and temperature sensitivity of TRPV1: effects of SNAP (300 μM) on pH (**h**) and temperature dependence (**i**) of responses mediated by TRPV1 and the mutant are shown (n = 7–50). $^*P < 0.05$ and $^{***}P < 0.001$, compared to TRPV1 in the absence of SNAP.

(**Fig. 8b,c**). Thus, heteromultimeric TRPC5/TRPC1 and TRPC5/TRPC4 channels are likely to conduct native NO-activated Ca^{2+} influx in endothelial cells.

ATP is a vasodilator that activates G protein–coupled receptors, which results in endothelial NO production via eNOS (ref. 16). We tested whether the NO produced by this physiological stimulation activates Ca^{2+} influx in BAEC. ATP induced $[Ca^{2+}]_i$ rises due to Ca^{2+} release in the absence of extracellular Ca^{2+} and those due to Ca^{2+} influx after the readmission of external Ca^{2+} (**Fig. 9d**). The NOS inhibitor N^{ω}-nitro-L-arginine methylester (L-NAME, **14**) failed to affect Ca^{2+} release but significantly ($P < 0.001$) suppressed the Ca^{2+} influx (**Fig. 9d**) and NO production (**Supplementary Fig. 5**).

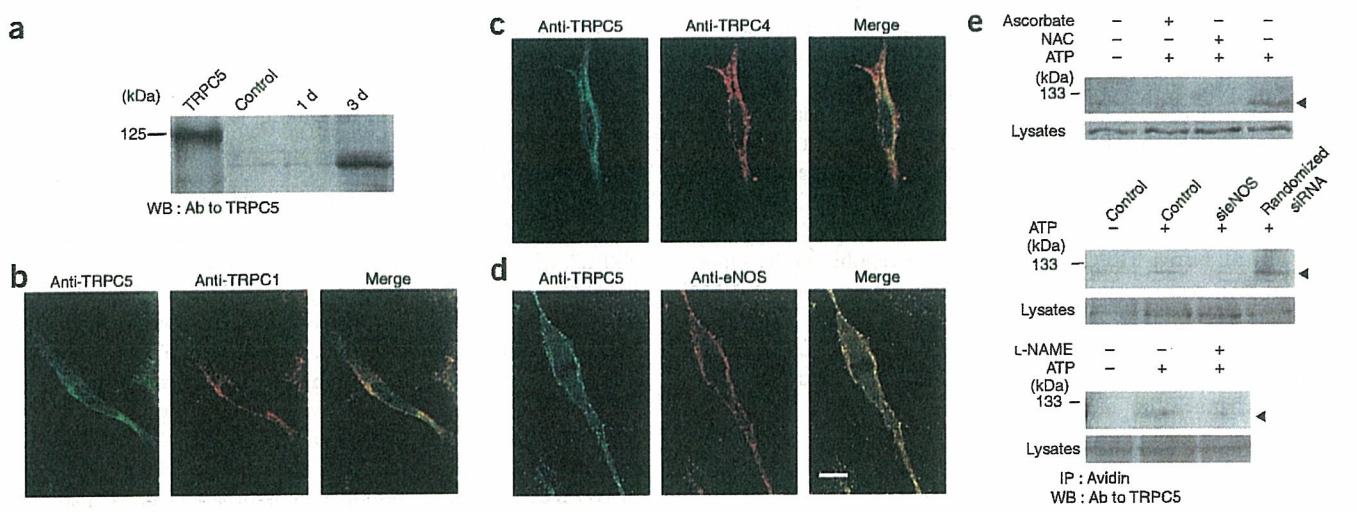

Figure 8 Physiological S-nitrosylation of native TRPC5 proteins in cultured endothelial cells. (**a**) WB reveals that TRPC5 protein expression is enhanced after a 3-d culture in BAEC. (**b–d**) Confocal fluorescence immunoimages of TRPC5 (green), TRPC1 (**b**), TRPC4 (**c**) and eNOS (**d**) (all red), and overlay of images (yellow) in BAECs. The bar indicates 10 μm. (**e**) S-nitrosylation of native TRPC5 by ATP receptor stimulation, and its inhibition by NAC and ascorbate (top), sieNOS (middle) and L-NAME (bottom) in BAECs.

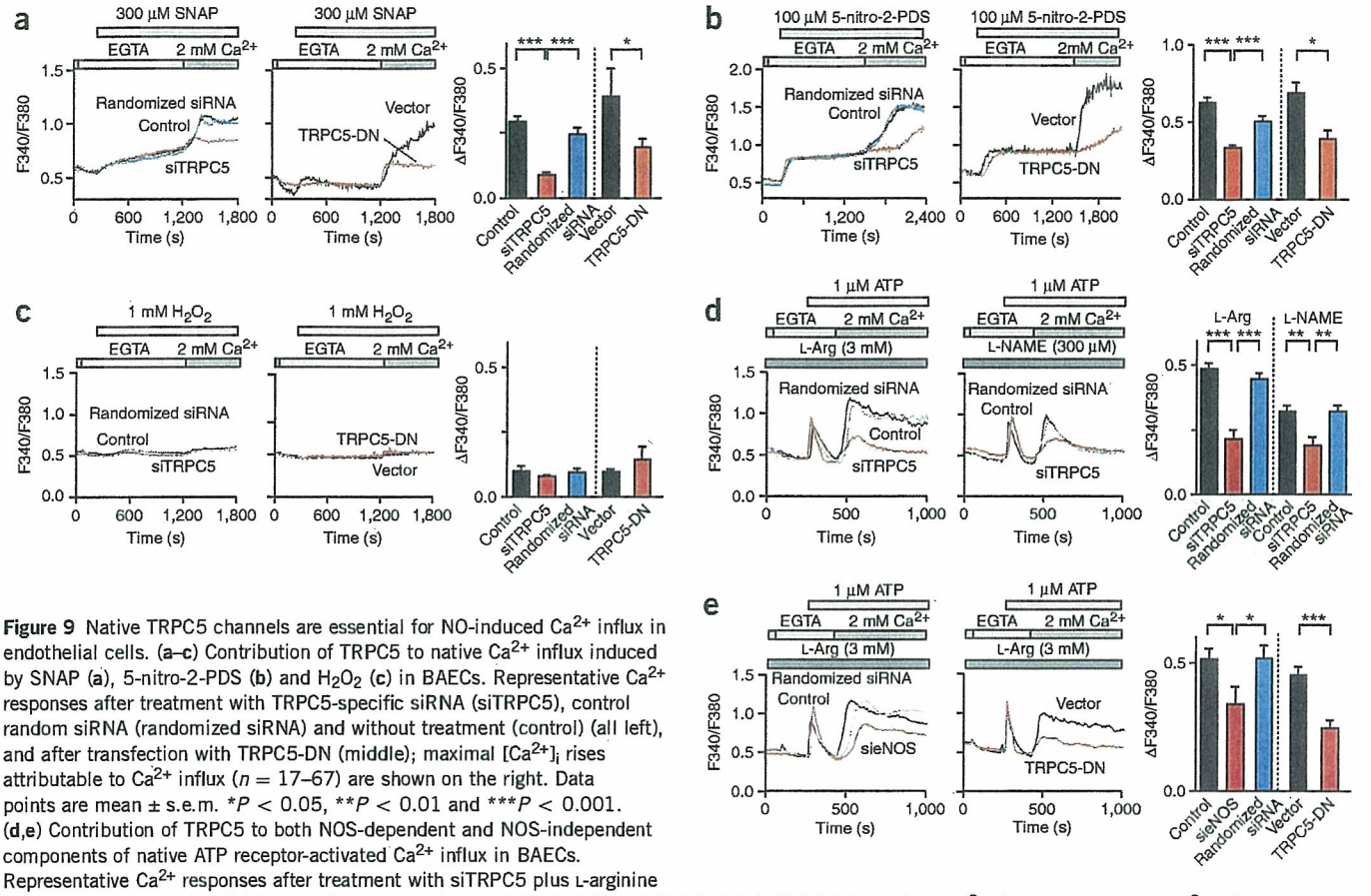

Figure 9 Native TRPC5 channels are essential for NO-induced Ca^{2+} influx in endothelial cells. (**a–c**) Contribution of TRPC5 to native Ca^{2+} influx induced by SNAP (**a**), 5-nitro-2-PDS (**b**) and H_2O_2 (**c**) in BAECs. Representative Ca^{2+} responses after treatment with TRPC5-specific siRNA (siTRPC5), control random siRNA (randomized siRNA) and without treatment (control) (all left), and after transfection with TRPC5-DN (middle); maximal $[Ca^{2+}]_i$ rises attributable to Ca^{2+} influx (n = 17–67) are shown on the right. Data points are mean ± s.e.m. $^*P < 0.05$, $^{**}P < 0.01$ and $^{***}P < 0.001$. (**d,e**) Contribution of TRPC5 to both NOS-dependent and NOS-independent components of native ATP receptor-activated Ca^{2+} influx in BAECs. Representative Ca^{2+} responses after treatment with siTRPC5 plus L-arginine (left) and L-NAME (middle) (**d**), and after suppression by sieNOS (left) and TRPC5-DN (middle) (**e**); maximal Ca^{2+} rises attributable to Ca^{2+} influx (**d**, n = 50–94; **e**, n = 21–38) are shown on the right. $^*P < 0.05$, $^{**}P < 0.01$ and $^{***}P < 0.001$.

This result, together with similar effects elicited by eNOS-targeted siRNA (sieNOS) (**Fig. 9e** and **Supplementary Fig. 5**) and by NO quencher *N*-acetyl-L-cysteine (NAC, **15**) and *S*-nitrosocysteine-selective reducing agent ascorbate (**Supplementary Fig. 5**), indicates a critical role for endogenous eNOS in inducing ATP receptor–activated Ca^{2+} influx. siTRPC5 more extensively diminished the Ca^{2+} influx and abolished the L-NAME sensitivity (**Fig. 9d**), which suggests that TRPC5 is essential for Ca^{2+} influx activated by NO via eNOS upon receptor stimulation. TRPC5-DN, which can also exert a suppressive effect on Ca^{2+} influx via nitrosylated TRPC5 (**Supplementary Fig. 1**), similarly suppressed the Ca^{2+} influx (**Fig. 9e**). In BAEC, siTRPC5 by contrast revealed lack of involvement of TRPC5 in SOC (**Supplementary Fig. 5**). Native TRPC5 proteins were susceptible to the suppression of ATP receptor–induced nitrosylation by ascorbate, L-NAME, NAC and sieNOS (**Fig. 8e** and **Supplementary Fig. 5**). Furthermore, confocal immunoimages indicate localization of TRPC5 with eNOS (**Fig. 8d**). These results provide evidence for activation of native TRPC5 channels by nitrosylation via eNOS upon ATP receptor stimulation in endothelial cells.

DISCUSSION

The present study describes a previously unknown activation mechanism of TRP channels via cysteine S-nitrosylation, as well as a structural motif essential for the activation gating. Among TRPCs coupled to PLC-linked receptors, TRPC5 showed prominent sensitivity to NO, and nitrosylated Cys553 and Cys558 mediated the responsiveness in TRPC5. A critical contribution of native nitrosylated TRPC5 to Ca^{2+} entry was revealed by siRNA and dominant negative suppression in endothelial cells. Notably, TRPC1 and TRPC4β associated with TRPC5, and thermosensors TRPV1, TRPV3 and TRPV4, which have cysteines nearby the same putative pore-forming region, responded well to NO. These TRPC and TRPV channels may comprise a new TRP protein category whose members serve as ubiquitous cell-surface NO sensors that are essential for integrating NO and Ca^{2+} signals.

The data (**Fig. 4**) suggest that NO and reactive disulfides exert their actions independently of receptor-induced cascades or Ca^{2+} store depletion in activating TRPC5. In fact, SNAP (at low concentrations) and reactive disulfides failed to activate TRPC2, TRPC3, TRPC6 and TRPC7, which are all activated by receptor stimulation[2–7]. SNAP also failed to significantly affect endogenous SOCs in HEK cells (**Supplementary Fig. 1**). The abolishment of DTNB-2Bio incorporation by SNAP co-application and by the C553S TRPC5 mutation, and the suppression of nitrosylation by the C553S mutation (**Fig. 5**), further indicate that both NO and reactive disulfides directly modify Cys553 in the TRPC5 protein. Compared to C553S, C558S weakly reduced nitrosothiol concentrations. This, together with the partial resistance of NO-induced TRPC5 response to ascorbate (**Fig. 3a**) may suggest that the free sulfhydryl group of Cys558 nucleophilically attacks nitrosylated Cys553 to form a disulfide bond that stabilizes the open state. S-nitrosylation activates the ryanodine receptor channel[37] and cyclic nucleotide-gated cation channels[38], and it modulates NMDA receptors[33]. Ryanodine receptors are also activated by reactive

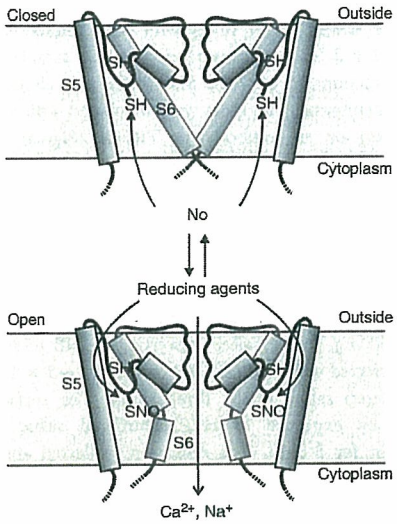

Figure 10 Model for TRP channel activation by NO and reactive disulfides. Possible protein conformation change during activation of TRPC5 channels by NO is shown. The activation trigger NO modifies the free sulfhydryl group of Cys553 that is accessible from the cytoplasmic side. This direct thiol S-nitrosylation induces a bend of S6 that opens the intracellular activation gate. The cysteine modification is reversed by the hydrophilic reducing agents DTT and ascorbate applied externally. SNO, *S*-nitrosothiol.

disulfides[12]. In proteins with high NO sensitivity, basic and acidic amino acids surrounding S-nitrosylated cysteines[11] have been proposed to enhance the nucleophilicity of sulfhydryl and its S-nitrosylation, as reported in acid-base catalysis of hemoglobin nitrosylation. In this context, charged residues flanking Cys553 and Cys558 (**Fig. 6a**) may confer modification susceptibility to their free sulfhydryls and to the free sulfhydryls of their counterpart cysteines in TRPC and TRPV channels, which are commonly distinguished on the basis of their characteristic activation triggers: receptor activation and heat, respectively. Notably, so-called thermoTRPs are comprised of members of several TRP protein families (TRPV, TRPM and TRPA)[3–5]. Therefore, together with NO-activated TRP proteins, thermoTRPs[3–5] can be considered as one of the few functional categories that extends over several TRP protein families. Our findings may provide the first clear chemical biological basis for TRP categorization of this hierarchy.

Our results suggest that NO and reactive disulfides selectively modify Cys553 and Cys558 residues that are coupled to the gating apparatus in functionally critical domains of the TRPC5 protein. Because C553S and C558S mutations of TRPC5 only partially suppress receptor-induced TRPC5 responses (**Supplementary Fig. 4**), the cysteines are not absolute necessities but probably have an important regulatory role in TRPC5 activation. Intact receptor-induced responses after DTT treatment (unpublished data) further suggest that the oxidative cysteine modifications are not required for receptor stimulation to activate TRPC5. In TRPV1, the cysteine mutation that impaired NO sensitivity failed to affect H^+ and temperature sensitivities under the control condition in the absence of NO. Therefore, the role played by the nitrosylation-target cysteines in H^+- and heat-induced activation of TRPV1 may be qualitatively comparable to the regulatory role played by the counterpart cysteines in receptor-induced activation of TRPC5, assuming quantitative differences between the mutations in severity of functional impairments attributable to structural changes.

Surprisingly, despite the location of Cys553 and Cys558 in the extracellularly disposed S5-S6 linker (according to previous studies[34]), the modifications are unlikely to affect the structure of the ion-conducting pore, as similar single-channel conductances are observed for the spontaneously activated TRPC5 channel (47.6 pS)[39] and the 5-nitro-2-PDS–activated TRPC5 channel (44.1 pS). Moreover, the sidedness of action of DTNB and the time lags preceding the responses after agent application support the hypothesis that modification agents access from the cytoplasmic side to open the intracellular activation gate of TRPC5 channels (**Fig. 10**). In *D. melanogaster* Shaker voltage-gated K^+ channels, the activation gate formed by S6 residues near the intracellular entrance of the pore cavity has been identified[31]. Considering the longer S5-S6 linkers of TRPC5, TRPC1 and TRPC4, which are comprised of approximately 60 residues (in comparison with 50 residues in TRPC2, TRPC3, TRPC6 and TRPC7 and 40 residues in the Shaker K^+ channel), the TRPC5 S5-S6 linker with modified Cys553 may be invaginated toward the cytoplasm to reach the S6 activation gate (**Fig. 10**). However, external DTT and ascorbate reversed the TRPC5 activation (**Fig. 3a,b** and **Supplementary Fig. 2**), and in TRPV1 the cysteine counterparts have been suggested as sites for blockade by externally applied oxidizing agents[40,41]; also, an antibody raised against a peptide containing Cys553 at the C terminus inhibits TRPC5 activity[42]. Therefore, Cys553 is very likely located at the interface between the inside and outside of the cell.

The plasma-membrane expression of TRPC5 unaffected by C553S, C558S or cellular stimulations except epidermal growth factor (**Supplementary Fig. 4**) may suggest minimal contribution of protein trafficking to NO-induced activation in HEK cells. However, involvements of protein recruitments through the fusion of vesicles with the plasma membrane and lateral movements within the plasma membrane cannot be excluded. Ca^{2+}-dependent BK-type K^+ channels are modulated by several mechanisms, such as redox-sensitive extracellular gates containing cysteine residues in the auxiliary β subunit[43] and heme bound to the pore-forming α subunit[44]. Therefore, conformational changes elicited by cysteine modification in an unidentified associated protein may be transmitted to TRPC5 via Cys553, if the protein association is maintained during the labeling assays. Thus, cysteine modifications may exert their action via multiple pathways on the pore-forming TRPC5 protein, which is consistent with the previously reported multiplicity of signals responsible for channel activation of TRPC5 (ref. 45).

Ca^{2+} influx via nitrosylated TRP channels may mediate the positive feedback regulation of Ca^{2+}-dependent NO production. In support of this view, native NO-activated Ca^{2+} channels have been reported in different systems including endothelial cells[24,25,46,47], in which cation currents are activated by glutathione disulfide[48]. However, suppressive effects of NO on Ca^{2+} entry have also been demonstrated in endothelial cells[26,27]. This discrepancy is at least in part attributable to diversity in NO susceptibility of ion channels and signaling pathways that regulate Ca^{2+} influx. In fact, Ca^{2+} entry via SOCs is potentiated indirectly by NO through the enhancement of Ca^{2+} release[23]. In endothelial cells in which cGMP mediates NO signals (for example, as observed in smooth muscle[26,27]), NO suppresses Ca^{2+} entry. Moreover, NO has been shown to inhibit NOS[11]. Thus, ensembles of multiple NO-regulated mechanisms may determine net Ca^{2+} entry. Notably, in the NMDA receptor Ca^{2+}-permeable channel NR1/NR2A, nNOS physically coupled to the NR1 subunit through the scaffolding protein PSD-95 nitrosylates the NR2A subunit to elicit feedback inhibition of channel activity[33]. To resolve the complexity in cross talk between NO and Ca^{2+} signals, precise identification of physiological protein interaction between nitrosylated TRP channels and NOSs is necessary.

Our immunolocalization studies have revealed that TRPC5 is distributed on both the apical and basal membranes in the endothelial cell layer of vascular tissue (unpublished data). Given that vasodilator receptors are distributed at the apical luminal surface of endothelial cell layers, NO that is initially produced there may diffuse across the cytoplasm and activate TRPC5 proteins located at the basolateral membrane. This may lead to an efficient propagation of Ca^{2+} signals vectorized toward the basal membrane. The feedback mechanism may further contribute to global $[Ca^{2+}]_i$ rises or oscillations and to full activation of eNOS at the Golgi in endothelial cells, thereby leading to synchronization of neighboring smooth muscle cells in vascular relaxation. Notably, TRPC5 is important in neurite extension[36]. Given that NO signals are reported to regulate neurite extension[49], the feedback mechanism may also be important in growth-cone morphology. In terms of TRPVs, our results may raise the possibility that nitrosylation-induced Ca^{2+} entry is involved in heat or pain sensation. Thus, the positive feedback regulation of Ca^{2+} signals by NO-activated TRP channels may be involved in diverse biological systems.

Impaired aortic vasorelaxation and reduced endothelial $[Ca^{2+}]_i$ increase upon agonist stimulation has been demonstrated in TRPC4-deficient mice[50]. These results are notable in the context of our study, considering that Cys553 and Cys558 counterparts are found in TRPC4. TRPC5/TRPC4β and TRPC5/TRPC1 channels had intact NO sensitivity and significant H_2O_2 resistance. These observations, together with our immunohistochemistry and co-immunoprecipitation experiments (**Figs. 6** and **8**), suggest that heteromultimerization with TRPC1 or TRPC4β may enable TRPC5 to maintain its NO-sensing function while acquiring resistance to the pathological action of reactive oxygen species[11,28] in endothelial cells. To understand the mechanism underlying this sensitivity, three-dimensional structural analysis and detailed studies of the binding pocket for the activation triggers using cysteine-modification agents of different sizes is critical.

METHODS

Cell culture and cDNA expression. The TRPC5 mutants were constructed using PCR techniques. TRPC1-Flag and TRPC5-Flag were first established in plasmid pCMV-Tag4 (Stratagene). The culture of HEK cells and chicken DT40 B lymphocytes, as well as cDNA expression, were performed as described previously[28,32]. BAECs were cultured in phenol red–free DMEM (Gibco) containing 10% FBS, 30 units ml^{-1} penicillin, 1 μM all-*trans*-retinoic acid and 30 μg ml^{-1} streptomycin at 37 °C under 5% CO_2. To remove retinoid hormones, FBS was incubated with 0.5% dextran-coated charcoal (Sigma) at 4 °C overnight. TRPC5-DN was transfected using Lipofectamine 2000 (Invitrogen). Cells were trypsinized and diluted by DMEM and plated onto glass coverslips 24 h after transfection. The cells were subjected to measurements 8–24 h after plating.

siRNA experiment. We used the sense siRNA sequences 5′-AATGCCTTCTCC ACGCTCTTT-3′ for bovine TRPC5 and 5′-AATATCCTGGAGGATGTGGCC-3′ for bovine eNOS. The randomized siRNA target sequences were 5′-AATCGC CTCTTACGCTCCTTT-3′ and 5′-AATGCGTGTTGCTAGACGCAG-3′, respectively. Computer analysis confirmed this sequence to be a specific target that does not have homology to other bovine genes. We used the Silencer siRNA Construction Kit (Ambion) to construct siRNA oligomers, and we transfected the siRNAs to cultured endothelial cells using Lipofectamine 2000.

Immunoprecipitation and western blot analysis. HEK cells (~3 × 10^6) transfected with TRPC4β with TRPC5-Flag, TRPC5-GFP with TRPC1-Flag, TRPC4β with pCMV-Tag4, and TRPC5-GFP with pCMV-Tag4 were lysed in 200 μl of RIPA buffer (pH 8.0) containing 150 mM NaCl, 1% Nonidet P-40, 0.5% sodium deoxycholate, 0.1% SDS, 50 mM Tris, 1 mM PMSF and 10 μg ml^{-1} leupeptin. TRPC5-Flag and TRPC1-Flag were immunoprecipitated with M2 monoclonal antibody to Flag (Sigma) in the presence of sepharose A-agarose beads (Amersham Pharmacia) rocked overnight at 4 °C. The immune complexes were washed eight times with RIPA buffer for 5 min at room temperature (22 ± 2 °C) and resuspended in SDS sample buffer. The protein samples were fractionated by 7.5% SDS-PAGE and electrotransferred onto a nitrocellulose membrane. The blots were incubated with an antibody to GFP (BD Biosciences) or an antibody to TRPC4 (Sigma) and stained using the enhanced chemiluminescence (ECL) system (Amersham Pharmacia). Cultured BAECs were subjected to western blot analysis using anti-mouse TRPC5 rabbit antiserum (H8C1) directed against the C terminus (682-CPKRDPDGRRRRHNLRS-698).

DTNB-2Bio labeling assay. DTNB-2Bio was synthesized by biotinylation of the two carboxyl groups of DTNB (Dojindo) using EZ-link 5-(Biotinamido) pentylamine (50 mg, Pierce) after converting DTNB to succinimidyl DTNB. HEK cells transfected with TRPC5-GFP or vector (~5 × 10^6) were washed by phosphate-buffered saline (PBS) three times. The surface membrane was permeabilized by exposure to HEPES-buffered saline (HBS) containing 0.01% digitonin for 5 min. The cells were collected and exposed to HBS containing 100 μM DTNB-2Bio for 20 min at room temperature. The cells were washed with PBS three times, harvested, and lysed in RIPA buffer. Cell lysates were incubated batch-wise with NeutrAvidin-Plus beads (Pierce) overnight at 4 °C with constant shaking. The beads were rinsed six times with RIPA buffer by centrifugation at 14,000 r.p.m. for 30 s. The proteins were eluted in sample buffer containing DTT (50 mM) at room temperature for 20 min and analyzed by 10% SDS-PAGE and western blot detection using an antibody to GFP.

S-nitrosylation assay. The S-nitrosylation assay (biotin switch assay) was performed as described previously[10] with a few modifications. HEK cells expressing TRPC5-GFP constructs were incubated with SNAP (5 mM) or with control DMSO in the dark at room temperature for 10 min, and BAECs were pretreated with ascorbate (10 mM), NAC (1 mM) for 15 min, or L-NAME (10 mM) for 32 h, and then exposed to ATP (1 μM) in the dark at room temperature for 5 min. The cells were washed with PBS two times, harvested, and lysed in RIPA buffer. The extracts were incubated with 100 mM methylmethanethiosulfonate (MMTS) and 2.5% SDS at 50 °C for 30 min, and MMTS was removed by precipitation with an equal volume of –30 °C acetone. After resuspending the proteins in HEN buffer (250 mM HEPES pH 7.7, 1 mM EDTA and 0.1 mM neocuproine) containing 1% SDS, we added sodium ascorbate (1 mM final concentration) and biotin-HPDP (1 mM final concentration, Pierce). The mixtures were incubated for 1 h at 25 °C in the dark with intermittent vortexing. Biotinylated nitrosothiols were then acetone-precipitated with 2 volumes of –30 °C acetone to remove residual biotin-HPDP. After centrifugation, the pellet was resuspended in 0.1 ml HEN buffer containing 1% SDS. Two volumes of neutralization buffer (20 mM HEPES, pH 7.7, 100 mM NaCl, 1 mM EDTA, 0.5% Triton X-100) were added, and biotinylated proteins were incubated with 20 μl of NeutrAvidin-Plus beads for 1 h at room temperature. The resin was extensively washed in 10 volumes of neutralization buffer containing 600 mM NaCl. The proteins were eluted in sample buffer containing DTT (50 mM) at room temperature for 30 min and analyzed by 7.5% SDS-PAGE and western blotting with an antibody to GFP to detect TRPC5-GFP or an antibody to TRPC5 (Alomone) to detect native bovine TRPC5.

Confocal immunovisualization in BAECs. Cultured BAECs were incubated for 1 h at room temperature with goat polyclonal antibody to TRPC5 (1:100) (Santa Cruz Biotech) plus each one of rabbit polyclonal antibodies to TRPC1 (1:100) (Sigma) and to TRPC4 (1:100) (Alomone), or plus mouse monoclonal antibody to eNOS (1:500) (Calbiochem) in PBS containing 5% BSA, and for 1 h with the fluorescein isothiocyanate (FITC)-conjugated anti-goat IgG to detect TRPC5, Cy3-conjugated anti-mouse IgG to detect eNOS and Cy3-conjugated anti-rabbit IgG to detect TRPC1 or TRPC4. The fluorescence images were acquired with a confocal laser-scanning microscope using the 488-nm line of an argon laser for excitation and a 505-nm to 525-nm band-pass filter for emission, or the 543-nm line of a HeNe laser for excitation and a 560-nm long-pass filter for emission. The specimens were viewed at high magnification using plan oil objectives (×60, 1.40 numerical aperture (NA), Olympus).

Fluorescent $[Ca^{2+}]_i$ measurements and electrophysiology. The fura-2 fluorescence was measured in HBS containing the following: NaCl, 107 mM; KCl,

6 mM; $MgSO_4$, 1.2 mM; $CaCl_2$, 2 mM; glucose, 11.5 mM; HEPES, 20 mM; adjusted to pH 7.4 with NaOH. The 340:380-nm ratio images were obtained on a pixel-by-pixel basis. Fura-2 measurements were carried out at 22 ± 1 °C using HBS adjusted to pH 7.4, or as otherwise stated. Whole-cell currents were recorded at room temperature using the conventional whole-cell mode of the patch clamp technique with EPC9 amplifier (Heka) as described previously[28]. The standard pipette-filling solution contained the following: CsOH, 105 mM; L-aspartate, 105 mM; CsCl, 40 mM; $CaCl_2$, 1.33 mM; $MgCl_2$, 2 mM; ethyleneglycol-bis(β-aminoethyl)-*N,N,N′,N′*-tetraacetic acid (EGTA, 16), 5 mM; HEPES, 5 mM; Na_2ATP, 2 mM; adjusted to pH 7.25 with CsOH (50 nM calculated free Ca^{2+}). The 2-mM Ca^{2+}-NaCl solution contained: NaCl, 125 mM; $MgCl_2$, 1.2 mM; $CaCl_2$, 2 mM; glucose, 10 mM; HEPES, 11.5 mM; mannitol, 49 mM; adjusted to pH 7.4 with NaOH. The osmolarity of external solutions was adjusted to about 325 mosM. For the inside-out patch recording, the recording pipette contained the 2-mM Ca^{2+}-NaCl solution, and the bathing solution had the same composition as standard pipette-filling solution. Recordings were filtered at 1 kHz. Linear regression was used to yield a single-channel conductance from *I–V* relationship.

Statistical analysis. All data are expressed as means ± s.e.m. The data were accumulated under each condition from at least three independent experiments. The statistical analyses were performed using the Student's *t*-test.

Additional methods. Further details of cell culture, complementary DNA expression, synthesis of DTNB-2Bio, confocal immunovisualization of proteins, and fluorescence and electrophysiological measurements are in **Supplementary Methods** online.

Accession codes. GenBank: bovine TRPC5, XM_617015; bovine eNOS, NM_181037.

Note: Supplementary information is available on the Nature Chemical Biology website.

ACKNOWLEDGMENTS

We thank D.E. Clapham and C. Strubing for TRPC5-DN, T. Furukawa and M. Nishida for helpful discussions, E. Mori and M. Sasaki for expert experiments and T. Kurosaki for IP_3 receptor–deficient DT40 cells. This study was supported by research grants from the Ministry of Education, Culture, Sports, Science and Technology of Japan, the Japan Society for the Promotion of Science, and from the Mitsubishi Foundation.

AUTHOR CONTRIBUTIONS

T.Y., acquisition, analysis and interpretation of data, and drafting and revision of the manuscript; N.T., S.Y., Y.H., R.I., T.M., M.T., S.S. and Y.S., acquisition, analysis and interpretation of data; Y.M., analysis and interpretation of data, and drafting and critical review of the manuscript.

COMPETING INTERESTS STATEMENT

The authors declare that they have no competing financial interests.

Published online at http://www.nature.com/naturechemicalbiology
Reprints and permissions information is available online at http://npg.nature.com/reprintsandpermissions/

1. Berridge, M.J., Bootman, M.D. & Lipp, P. Calcium—a life and death signal. *Nature* **395**, 645–648 (1998).
2. Montell, C., Birnbaumer, L. & Flockerzi, V. The TRP channels, a remarkably functional family. *Cell* **108**, 595–598 (2002).
3. Clapham, D.E. TRP channels as cellular sensors. *Nature* **426**, 517–524 (2003).
4. Voets, T., Talavera, K., Owsianik, G. & Nilius, B. Sensing with TRP channels. *Nat. Chem. Biol.* **1**, 85–92 (2005).
5. Clapham, D.E., Julius, D., Montell, C. & Schultz, G. International Union of Pharmacology. XLIX. Nomenclature and structure-function relationships of transient receptor potential channels. *Pharmacol. Rev.* **57**, 427–450 (2005).
6. Zhu, X. *et al. trp*, a novel mammalian gene family essential for agonist-activated capacitative Ca^{2+} entry. *Cell* **85**, 661–671 (1996).
7. Vazquez, G., Wedel, B.J., Aziz, O., Trebak, M. & Putney, J.W., Jr. The mammalian TRPC cation channels. *Biochim. Biophys. Acta* **1742**, 21–36 (2004).
8. Caterina, M.J. *et al.* The capsaicin receptor: a heat-activated ion channel in the pain pathway. *Nature* **389**, 816–824 (1997).
9. Patapoutian, A., Peier, A.M., Story, G.M. & Viswanath, V. Thermo TRP channels and beyond: mechanisms of temperature sensation. *Nat. Rev. Neurosci.* **4**, 529–539 (2003).
10. Jaffrey, S.R., Erdjument-Bromage, H., Ferris, C.D., Tempst, P. & Snyder, S.H. Protein S-nitrosylation: a physiological signal for neuronal nitric oxide. *Nat. Cell Biol.* **3**, 193–197 (2001).
11. Hess, D.T., Matsumoto, A., Kim, S.O., Marshall, H.E. & Stamler, J.S. Protein S-nitrosylation: purview and parameters. *Nat. Rev. Mol. Cell Biol.* **6**, 150–166 (2005).
12. Zaidi, N.F., Lagenaur, C.F., Abramson, J.J., Pessah, I. & Salama, G. Reactive disulfides trigger Ca^{2+} release from sarcoplasmic reticulum via an oxidation reaction. *J. Biol. Chem.* **264**, 21725–21736 (1989).
13. Moncada, S., Higgs, A. & Furchgott, R. International Union of Pharmacology nomenclature in nitric oxide research. *Pharmacol. Rev.* **49**, 137–142 (1997).
14. Venema, V.J. *et al.* Bradykinin stimulates the tyrosine phosphorylation and bradykinin B2 receptor association of phospholipase Cγ1 in vascular endothelial cells. *Biochem. Biophys. Res. Commun.* **246**, 70–75 (1998).
15. Zachary, I. & Gliki, G. Signaling transduction mechanisms mediating biological actions of the vascular endothelial growth factor family. *Cardiovasc. Res.* **49**, 568–581 (2001).
16. Koyama, T., Kimura, C., Park, S.J., Oike, M. & Ito, Y. Functional implications of Ca^{2+} mobilizing properties for nitric oxide production in aortic endothelium. *Life Sci.* **72**, 511–520 (2002).
17. Hutcheson, I.R. & Griffith, T.M. Central role of intracellular calcium stores in acute flow- and agonist-evoked endothelial nitric oxide release. *Br. J. Pharmacol.* **122**, 117–125 (1997).
18. Lantoine, F., Iouzalen, L., Devynck, M.A., Millanvoye-Van Brussel, E. & David-Dufilho, M. Nitric oxide production in human endothelial cells stimulated by histamine requires Ca^{2+} influx. *Biochem. J.* **330**, 695–699 (1998).
19. Lin, S. *et al.* Sustained endothelial nitric-oxide synthase activation requires capacitative Ca^{2+} entry. *J. Biol. Chem.* **275**, 17979–17985 (2000).
20. Yao, X. & Garland, C.J. Recent developments in vascular endothelial cell transient receptor potential channels. *Circ. Res.* **97**, 853–863 (2005).
21. Mungrue, I.N. & Bredt, D.S. nNOS at a glance: implications for brain and brawn. *J. Cell Sci.* **117**, 2627–2629 (2004).
22. Khan, S.A. & Hare, J.M. The role of nitric oxide in the physiological regulation of Ca^{2+} cycling. *Curr. Opin. Drug Discov. Devel.* **6**, 658–666 (2003).
23. Volk, T., Mäding, K., Hensel, M. & Kox, W.J. Nitric oxide induces transient Ca^{2+} changes in endothelial cells independent of cGMP. *J. Cell. Physiol.* **172**, 296–305 (1997).
24. Chen, J. *et al.* Autocrine action and its underlying mechanism of nitric oxide on intracellular Ca^{2+} homeostasis in vascular endothelial cells. *J. Biol. Chem.* **275**, 28739–28749 (2000).
25. Li, N., Sul, J.Y. & Haydon, P.G. A calcium-induced calcium influx factor, nitric oxide, modulates the refilling of calcium stores in astrocytes. *J. Neurosci.* **23**, 10302–10310 (2003).
26. Kwan, H.Y., Huang, Y. & Yao, X. Store-operated calcium entry in vascular endothelial cells is inhibited by cGMP via a protein kinase G-dependent mechanism. *J. Biol. Chem.* **275**, 6758–6763 (2000).
27. Dedkova, E.N. & Blatter, L.A. Nitric oxide inhibits capacitative Ca^{2+} entry and enhances endoplasmic reticulum Ca^{2+} uptake in bovine vascular endothelial cells. *J. Physiol. (Lond.)* **539**, 77–91 (2002).
28. Hara, Y. *et al.* LTRPC2 Ca^{2+}-permeable channel activated by changes in redox status confers susceptibility to cell death. *Mol. Cell* **9**, 163–173 (2002).
29. Aarts, M. *et al.* A key role for TRPM7 channels in anoxic neuronal death. *Cell* **115**, 863–877 (2003).
30. Okada, T. *et al.* Molecular cloning and functional characterization of a novel receptor-activated TRP Ca^{2+} channel from mouse brain. *J. Biol. Chem.* **273**, 10279–10287 (1998).
31. del Camino, D. & Yellen, G. Tight steric closure at the intracellular activation gate of a voltage-gated K^+ channel. *Neuron* **32**, 649–656 (2001).
32. Sugawara, H., Kurosaki, M., Takata, M. & Kurosaki, T. Genetic evidence for involvement of type 1, type 2 and type 3 inositol 1,4,5-trisphosphate receptors in signal transduction through the B-cell antigen receptor. *EMBO J.* **16**, 3078–3088 (1997).
33. Choi, Y.B. *et al.* Molecular basis of NMDA receptor-coupled ion channel modulation by S-nitrosylation. *Nat. Neurosci.* **3**, 15–21 (2000).
34. Vannier, B., Zhu, X., Brown, D. & Birnbaumer, L. The membrane topology of human transient receptor potential 3 as inferred from glycosylation-scanning mutagenesis and epitope immunocytochemistry. *J. Biol. Chem.* **273**, 8675–8679 (1998).
35. Chang, A.S., Chang, S.M., Garcia, R.L. & Schilling, W.P. Concomitant and hormonally regulated expression of *trp* genes in bovine aortic endothelial cells. *FEBS Lett.* **415**, 335–340 (1997).
36. Greka, A., Navarro, B., Oancea, E., Duggan, A. & Clapham, D.E. TRPC5 is a regulator of hippocampal neurite length and growth cone morphology. *Nat. Neurosci.* **6**, 837–845 (2003).
37. Xu, L., Eu, J.P., Meissner, G. & Stamler, J.S. Activation of the cardiac calcium release channel (ryanodine receptor) by poly-S-nitrosylation. *Science* **279**, 234–237 (1998).
38. Broillet, M.C. & Firestein, S. Direct activation of the olfactory cyclic nucleotide-gated channel through modification of sulfhydryl groups by NO compounds. *Neuron* **16**, 377–385 (1996).
39. Yamada, H. *et al.* Spontaneous single-channel activity of neuronal TRP5 channel recombinantly expressed in HEK293 cells. *Neurosci. Lett.* **285**, 111–114 (2000).
40. Jin, Y. *et al.* Thimerosal decreases TRPV1 activity by oxidation of extracellular sulfhydryl residues. *Neurosci. Lett.* **369**, 250–255 (2004).
41. Tousova, K., Susankova, K., Teisinger, J., Vyklicky, L. & Vlachova, V. Oxidizing reagent copper-*o*-phenanthroline is an open channel blocker of the vanilloid receptor TRPV1. *Neuropharmacology* **47**, 273–285 (2004).

42. Xu, S.Z. *et al.* Generation of functional ion-channel tools by E3 targeting. *Nat. Biotechnol.* **23**, 1289–1293 (2005).
43. Zeng, X.H., Xia, X.M. & Lingle, C.J. Redox-sensitive extracellular gates formed by auxiliary β subunits of calcium-activated potassium channels. *Nat. Struct. Biol.* **10**, 448–454 (2003).
44. Tang, X.D. *et al.* Haem can bind to and inhibit mammalian calcium-dependent Slo1 BK channels. *Nature* **425**, 531–535 (2003).
45. Zeng, F. *et al.* Human TRPC5 channel activated by a multiplicity of signals in a single cell. *J. Physiol. (Lond.)* **559**, 739–750 (2004).
46. van Rossum, D.B., Patterson, R.L., Ma, H.T. & Gill, D.L. Ca^{2+} entry mediated by store depletion, S-nitrosylation, and TRPC3 channels. *J. Biol. Chem.* **275**, 28562–28568 (2000).
47. Thyagarajan, B. *et al.* Expression of Trp3 determines sensitivity of capacitative Ca^{2+} entry to nitric oxide and mitochondrial Ca^{2+} handling: evidence for a role of Trp3 as a subunit of capacitative Ca^{2+} entry channels. *J. Biol. Chem.* **276**, 48149–48158 (2001).
48. Koliwad, S.K., Kunze, D.L. & Elliott, S.J. Oxidant stress activates a non-selective cation channel responsible for membrane depolarization in calf vascular endothelial cells. *J. Physiol. (Lond.)* **491**, 1–12 (1996).
49. Zhang, N., Beuve, A. & Townes-Anderson, E. The nitric oxide-cGMP signaling pathway differentially regulates presynaptic structural plasticity in cone and rod cells. *J. Neurosci.* **25**, 2761–2770 (2005).
50. Freichel, M. *et al.* Lack of an endothelial store-operated Ca^{2+} current impairs agonist-dependent vasorelaxation in TRP4–/– mice. *Nat. Cell Biol.* **3**, 121–127 (2001).

Available online at www.sciencedirect.com
SCIENCE DIRECT®
Phytomedicine 13 (2006) 401–411
Phytomedicine
www.elsevier.de/phymed

Screening of novel nuclear receptor agonists by a convenient reporter gene assay system using green fluorescent protein derivatives

T. Suzuki[a,b], T. Nishimaki-Mogami[a], H. Kawai[a], T. Kobayashi[a], Y. Shinozaki[a], Y. Sato[a], T. Hashimoto[c], Y. Asakawa[c], K. Inoue[a], Y. Ohno[a], T. Hayakawa[a], T. Kawanishi[a,*]

[a]*National Institute of Health Sciences, Tokyo, Japan*
[b]*Pharmaceuticals and Medical Device Agency, Tokyo, Japan*
[c]*Faculty of Pharmaceutical Sciences, Tokushima Bunri University, Tokushima, Japan*

Received 27 September 2004; accepted 6 April 2005

Abstract

Nuclear receptors represent a very good family of protein targets for the prevention and treatment of diverse diseases. In this study, we screened natural compounds and their derivatives, and discovered ligands for the retinoic acid receptors (RARs) and the farnesoid X receptor (FXR). In the reporter assay systems of nuclear receptors presented here, two fluorescent proteins, enhanced yellow fluorescent protein (EYFP) and enhanced cyan fluorescent protein (ECFP), were used for detection of a ligand-based induction and as an internal control, respectively. By optimizing the conditions (e.g., of hormone response elements and promoter genes for reporter plasmids), we established a battery of assay systems for ligands of RARs, retinoid X receptor (RXR) and FXR. The screening using the reporter assay system can be carried out without the addition of co-factors or substrates. As a result of screening of more than 140 compounds, several compounds were detected which activate RARs and/or FXR. Caffeic acid phenylethyl ester (CAPE), known as a component of propolis from honeybee hives, and other derivatives of caffeic acid up-regulated the expression of reporter gene for RARs. Grifolin and ginkgolic acids, which are non-steroidal skeleton compounds purified from mushroom or ginkgo leaves, up-regulated the expression of the reporter gene for FXR.

Keywords: FXR; RAR; Reporter assay; Fluorescence; GFP; Caffeic acid; Ginkgolic acid; Grifolin

Introduction

Nuclear hormone receptors are ligand-activated transcription factors that are involved in a variety of physiological, developmental, and toxicological processes. The nuclear hormone receptor superfamily includes receptors for thyroid and steroid hormones, retinoids and vitamin D, as well as receptors for unknown ligands. These receptors share a highly conserved DNA-binding domain and a discrete ligand-binding domain, and bind to hormone response elements (HREs) on the DNA during the formation of homodimers, heterodimers, or monomers. This ligand binding to nuclear receptors leads to conformational

*Corresponding author. Tel.: +81 3 3700 9064; fax: +81 3 3700 9084.
E-mail address: kawanish@nihs.go.jp (T. Kawanishi).

0944-7113/$ - see front matter © 2005 Elsevier GmbH. All rights reserved.
doi:10.1016/j.phymed.2005.09.003